Report

Cell Reports

Proteomics of Cytochrome *c* Oxidase-Negative versus -Positive Muscle Fiber Sections in Mitochondrial Myopathy

Graphical Abstract

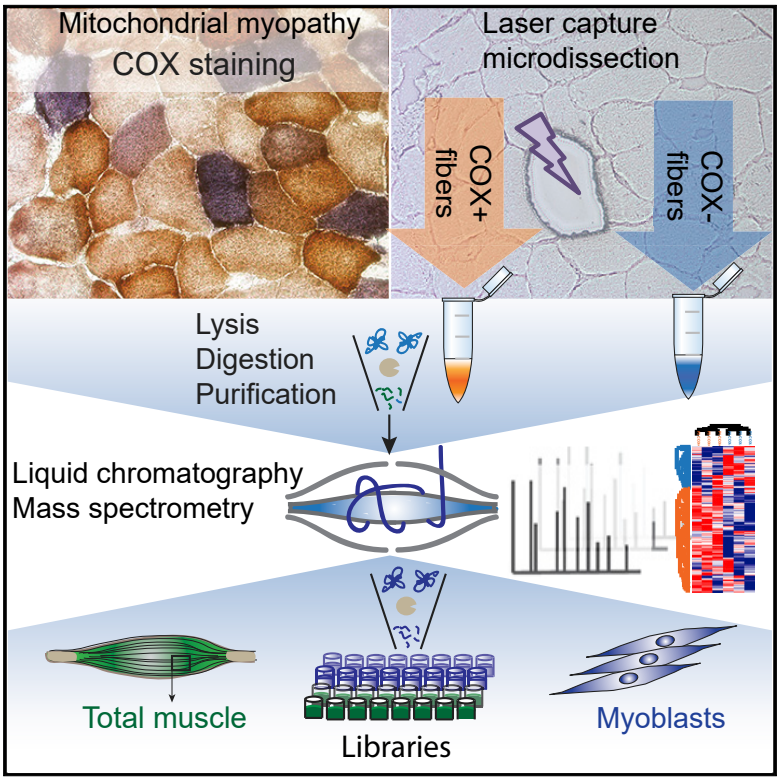

Highlights

- Laser capture microdissection enables single muscle fiber proteomics
- COX^+ and COX^- muscle fibers display different proteomic profiles
- COX^- fibers upregulate mitochondrial ribosomes, translation proteins, and chaperones
- Data reveal compensatory mechanisms in muscle fibers struggling with energy shortage

Authors

Marta Murgia, Jing Tan, Philipp E. Geyer, Sophia Doll, Matthias Mann, Thomas Klopstock

Correspondence

mmann@biochem.mpg.de (M.M.), tklopsto@med.lmu.de (T.K.)

In Brief

Murgia et al. use mass spectrometry-based proteomics to dissect the pathological mosaicism of compensated COX^+ fibers and decompensated COX^- fibers in mitochondrial myopathy. On this single-cell level, COX^- fibers show protean adaptive responses. These findings reveal compensatory mechanisms in muscle fibers struggling with energy shortage and metabolic stress.

Murgia et al., 2019, Cell Reports *29*, 3825–3834
December 17, 2019
https://doi.org/10.1016/j.celrep.2019.11.055

CellPress

Cell Reports
Report

Proteomics of Cytochrome *c* Oxidase-Negative versus -Positive Muscle Fiber Sections in Mitochondrial Myopathy

Marta Murgia,[1,2] Jing Tan,[3] Philipp E. Geyer,[1] Sophia Doll,[1] Matthias Mann,[1,4,*] and Thomas Klopstock[3,5,6,7,*]
[1]Department of Proteomics and Signal Transduction, Max Planck Institute of Biochemistry, Am Klopferspitz 18, 82152 Martinsried, Germany
[2]Department of Biomedical Sciences, University of Padova, Via Ugo Bassi, 58/B, 35131 Padua, Italy
[3]Friedrich Baur Institute, Department of Neurology, University of Munich, 80336 Munich, Germany
[4]NNF Center for Protein Research, University of Copenhagen, Blegdamsvej 3B, 2200 Copenhagen, Denmark
[5]German Center for Neurodegenerative Diseases (DZNE), Munich, Germany
[6]Munich Cluster for Systems Neurology (SyNergy), Munich, Germany
[7]Lead Contact
*Correspondence: mmann@biochem.mpg.de (M.M.), tklopsto@med.lmu.de (T.K.)
https://doi.org/10.1016/j.celrep.2019.11.055

SUMMARY

The mosaic distribution of cytochrome *c* oxidase$^+$ (COX$^+$) and COX$^-$ muscle fibers in mitochondrial disorders allows the sampling of fibers with compensated and decompensated mitochondrial function from the same individual. We apply laser capture microdissection to excise individual COX$^+$ and COX$^-$ fibers from the biopsies of mitochondrial myopathy patients. Using mass spectrometry-based proteomics, we quantify >4,000 proteins per patient. While COX$^+$ fibers show a higher expression of respiratory chain components, COX$^-$ fibers display protean adaptive responses, including upregulation of mitochondrial ribosomes, translation proteins, and chaperones. Upregulated proteins include C1QBP, required for mitoribosome formation and protein synthesis, and STOML2, which organizes cardiolipin-enriched microdomains and the assembly of respiratory supercomplexes. Factoring in fast/slow fiber type, COX$^-$ slow fibers show a compensatory upregulation of beta-oxidation, the AAA$^+$ protease AFG3L1, and the OPA1-dependent cristae remodeling program. These findings reveal compensatory mechanisms in muscle fibers struggling with energy shortage and metabolic stress.

INTRODUCTION

Mitochondrial disorders are multisystem diseases characterized by defective assembly and function of the respiratory chain. Mutations of both mtDNA and nuclear DNA (nDNA) are leading causes of these disorders, for a total prevalence of adult mitochondrial disease of 1 in 4,300 (Gorman et al., 2015). The human mitochondrial genome consists of 37 genes encoding 13 key proteins of the respiratory chain, 2 rRNAs, and 22 mitochondrial tRNAs (Schon et al., 2012). The vast majority of mitochondrial proteins are, however, encoded by the nDNA, which is why the corresponding disorders are inherited in a dominant, recessive, or X-linked manner (Spinazzola and Zeviani, 2009). Age-associated neurodegeneration, as in Parkinson and Alzheimer disease, as well as aging itself, has been associated with mitochondrial dysfunction (Lightowlers et al., 2015). Next-generation sequencing has extended the repertoire and greatly improved the diagnosis of mitochondrial disorders (Alston et al., 2017), but the underlying pathophysiological mechanisms are still poorly understood.

In most mtDNA-associated diseases, such as chronic progressive external ophthalmoplegia (CPEO), mitochondrial encephalomyopathy with lactic acidosis and stroke-like episodes (MELAS), and myoclonus epilepsy with ragged red fibers (MERRFs), skeletal muscle shows a pathological mosaicism at the level of its single cellular units, muscle fibers. This is apparent using the combined cytochrome *c* oxidase/succinate dehydrogenase (COX/SDH) histochemical staining, a common diagnostic test. Decompensated fibers are COX$^-$ but retain the blue SDH stain, which reflects the activity of complex II, the only respiratory complex entirely encoded by nDNA, and is thus unaffected by mutations of mtDNA. Compensated COX$^+$ fibers stain brownish as a result of preserved COX function (Figure 1A). The transition from the COX$^+$ to the COX$^-$ state depends on the proportion of mutant versus wild-type mtDNA in the fiber (heteroplasmy), the threshold being mutation dependent but mostly ~60% mutant mtDNA (Alston et al., 2017).

This pathological mosaicism is superimposed onto the physiological mosaic of different fiber types, which characterizes human skeletal muscle, one slow and two fast (2A and 2X), each with specific contractile and metabolic properties. In humans, slow fibers have more mitochondria than do fast fibers (Murgia et al., 2017).

Here, we investigated how mitochondrial disease alters the fiber proteome and how different fiber types cope with compromised respiratory chain activity. The mosaicism of COX$^+$ and COX$^-$ fibers offers the unique opportunity to investigate disease mechanisms at the cellular level. To this aim, we generated a proteomic workflow for a rapid, robust, and deep analysis of fiber heterogeneity from patient biopsies using laser capture microdissection (LCM) to separate COX$^+$ and COX$^-$ fibers (Figure 1A). Examples of a combination of LCM with proteomics

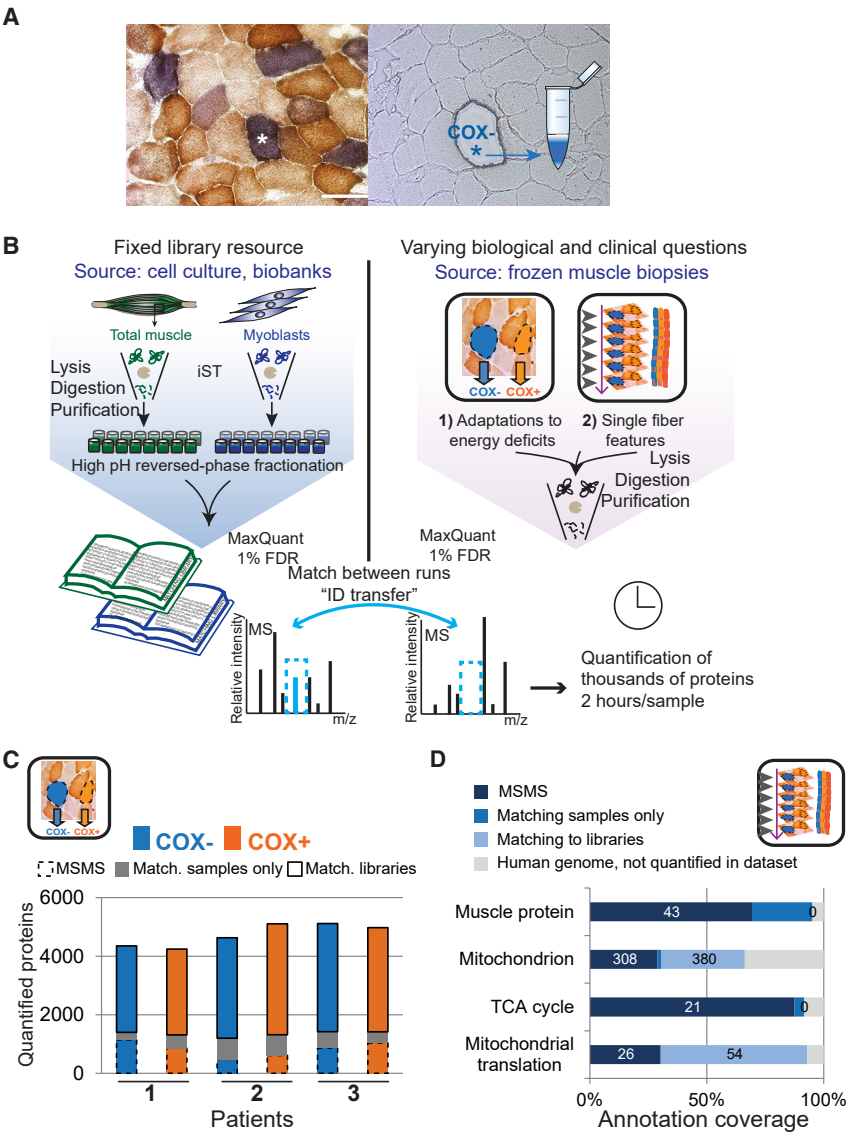

Figure 1. Proteomic Workflow for the Analysis of Muscle Biopsies in Mitochondrial Diseases

(A) Left panel, mosaic of COX^+ fibers (brown) and COX^- fibers (blue). The COX^- fiber labeled with an asterisk is re-identified in an unstained serial section and laser captured (right panel). Bar, 100 μm.

(B) Muscle biopsies (right panel) and pooled samples for library generation (left panel) are processed in parallel based on the in-StageTip (iST) protocol (Kulak et al., 2017). Patient samples are directly measured, library samples are fractionated to generate the "matching library" before liquid chromatography-(LC)-MS/MS.

(C) Proteins quantified in the dataset, illustrating the gain obtained by matching to the libraries or between samples only (match samples).

(D) Coverage of different mitochondrial annotations (GO) in the single-fibers dataset, expressed as the percentage of corresponding terms annotated in the human genome (protein numbers are shown in the bar segments).

See also Figures S1 and S2 and Tables S1, S2, and S3.

exist in the literature in other types of myopathies, such as filaminopathies, desminopathies, and other myofibrillar myopathies (Feldkirchner et al., 2013; Kley et al., 2013; Maerkens et al., 2013). Exploiting recent advances in sample preparation and proteomic technology applied to skeletal muscle (Kulak et al., 2014), we quantify >2,000 proteins from 20 individual fiber cryosections and >4,000 per patient (see Figure S1), uncovering fiber type-specific adaptive responses to disease, which would not be distinguishable in a total lysate.

RESULTS

Workflow for the Proteomic Analysis of Muscle Biopsies in Mitochondrial Disorders

We fractionated human muscle lysate and cultured myoblasts using a recently described "loss-less" nano-fractionator (Kulak et al., 2017). The resulting peptide libraries allowed us to overcome the dynamic range of the skeletal muscle proteome. Using the "match between runs" feature of the MaxQuant software (Cox and Mann, 2008; Tyanova et al., 2016a), we transferred identifications from the peptide libraries to the patients' samples (Figure 1B) (Deshmukh et al., 2015). We then optimized sample preparation in a single reaction vessel to minimize sample loss, contamination, and handling time (Kulak et al., 2014). We could measure >4,000 proteins per patient and 2,440 ± 350 proteins on average in single fibers (Figures 1C and S1A; Table S1).

Fractions separation yielded approximately 75% of all peptides in ≤4 fractions and up to 25% in 1 fraction (Figure S1B). We quantified 5,200 proteins (42,000 peptides) in the lysate, spanning >7 orders of magnitude. The most intense quartile was specifically enriched in myosin and ATP synthase complexes and the least intense in exosome and RNA-processing proteins (Figure S1C; Table S2). The myoblast lysate yielded 8,600 proteins (74,600 peptides), with gluconeogenesis and proteasome annotations enriched in the first quartile and DNA recombinase annotations in the last quartile. Myoblasts had higher proteome coverage than muscle lysate due to lower proteome dynamic range (Figures S1C and S1D; Table S3; Deshmukh et al., 2015).

Abundant proteins, such as those of the respiratory chain and the tricarboxylic acid (TCA) cycle, were directly identified by tandem mass spectrometry (MS/MS), whereas potentially disease-relevant protein classes such as those of mitochondrial translation reached high coverage (93%) only through matching to the libraries (Figure 1D).

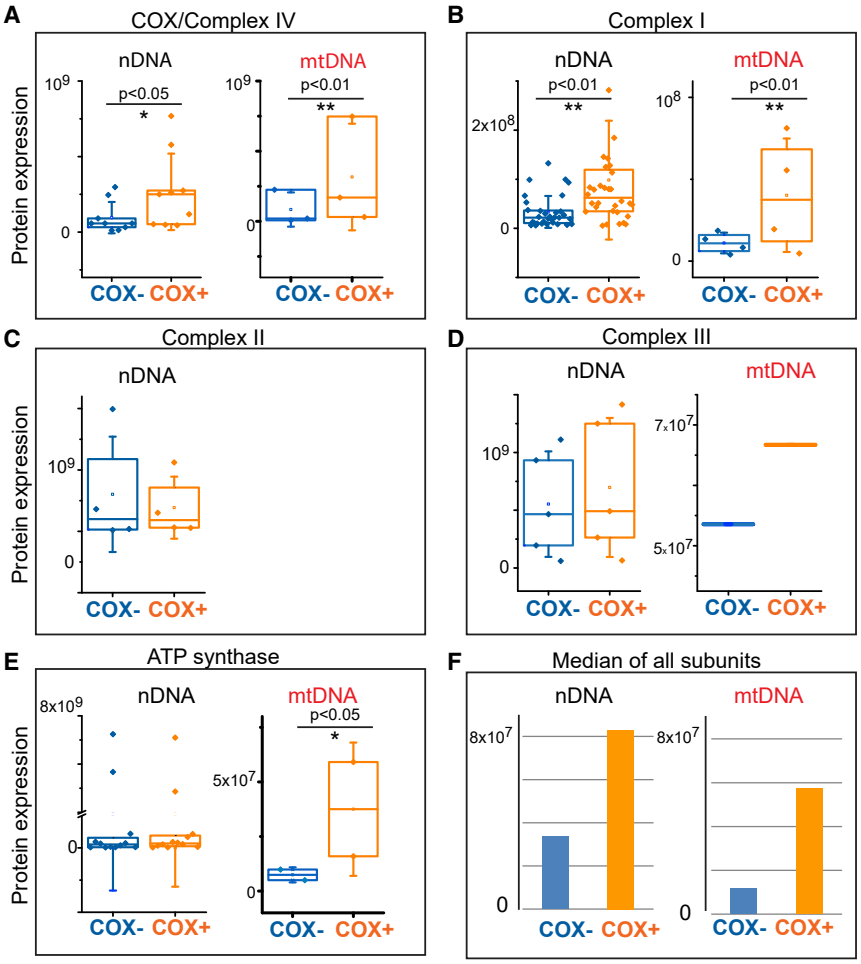

Figure 2. Expression of Respiratory Chain Complexes in COX$^+$ and COX$^-$ Fibers

The subunits of each complex were subdivided based on gene localization in nDNA (left) or mtDNA (right). The statistical significance was determined for each protein in 3 technical replicates of 3 patients by Student's t test. Complexes with a majority of subunits with significant expression differences report the p value indicated by *p < 0.05 or **p < 0.01. Boxplots are superimposed onto the mean of individual proteins. Boxes the show median and 25th and 75th percentiles; whiskers show the SDs. Protein expression shows LFQ values.

(A) Expression of COX subunits.

(B) Expression of complex I subunits.

(C) Expression of complex II subunits (all nDNA encoded).

(D) Expression of complex III subunits.

(E) Expression of ATP synthase subunits.

(F) Median expression of all respiratory chain subunits encoded by nDNA and mtDNA in 3 patients. Values represent the analysis of technical triplicates of 3 subjects.

See also Figures S3 and S4.

Technical replicates showed Pearson correlation coefficients of 0.98 (Figure S2). Pooled COX$^+$ and COX$^-$ fibers of the same individual (yellow squares) showed higher correlation (0.88–0.95) compared to those of different individuals (0.76–0.86). Correlations were on average lower in single fibers.

Expression of Respiratory Complexes and Mitochondrial Biogenesis Factors in COX$^+$ and COX$^-$ Fibers

Using LCM to cut individual fibers from 10-μm sections, we obtained separate pools of 100 COX$^+$ and 100 COX$^-$ fibers from each of 3 different patients (Figure 1A; Table S4). Pools of sections prevent sampling biases, such as different fiber type composition leading to different mitochondrial content (Table S5). We quantified 73 of 95 proteins Gene Ontology (GO) annotated to the respiratory chain and ATP synthase in humans. Classifying the respiratory chain subunits based on their gene localization in mtDNA and nDNA, we analyzed their expression in COX$^-$ and COX$^+$ fiber pools. Of 13 COX subunits quantified, 7 were significantly more abundant in COX$^+$ than in COX$^-$ fibers ($p < 0.05$), confirming that proteomics reads out the diagnostic histochemical difference (Figure S3). COX subunits encoded by mtDNA were significantly more expressed in COX$^+$ fibers ($p < 0.01$) (Figure 2A). For complex I, 24 of 45 subunits quantified were higher in COX$^+$ fibers than in COX$^-$ fibers ($p < 0.05$), with the 3 subunits of mtDNA origin displaying very high significance ($p < 10^{-4}$) (Figures 2B and S3). Three of 4 subunits of SDH/complex II, a histological marker of mitochondrial content, were also highly expressed in COX$^+$ (Figures 2C and S3). Four complex III subunits were more abundant in COX$^+$ than in COX$^-$ fibers, but overall the expression was similar. The mtDNA-encoded subunit MT-CYB was higher in COX$^+$ without reaching statistical significance (Figures 2D and S3). Complex V subunits encoded by nDNA were similarly expressed in the two groups, whereas we measured a large difference for the corresponding mtDNA-encoded ones (Figures 2E and S3). Overall, these results indicate that COX$^-$ fibers have a reduced expression of mtDNA-encoded proteins compared to COX$^+$ (Figure 2F). Accordingly, COX$^+$ fibers of CPEO patients were shown to contain more copies of mtDNA than COX$^-$ fibers (Greaves et al., 2010). We then looked at the assembly factors of mitochondrial complexes, which were slightly higher in COX$^-$ than in COX$^+$ fibers for all of the complexes but ATP synthase. Only 2 assembly factors of complex I (AIFM1, NDUFAF7) and 3 of complex IV (SCO1, COX15, COA7) showed significant differences ($p < 0.05$) (Figure S4A). Citrate synthase (CS), a classical marker of mitochondrial content, was 36% higher in COX$^-$ fibers (Figure S4B).

Next, we asked whether COX$^-$ fibers show increased mitochondrial biogenesis compared to COX$^+$ fibers, matching light and electron microscopy where signs of increased biogenesis (ragged red fibers [RRFs]) are more frequent and more marked in COX$^-$ than in COX$^+$ fibers (DiMauro and Schon, 2003). To this end, we curated a list of human proteins involved in

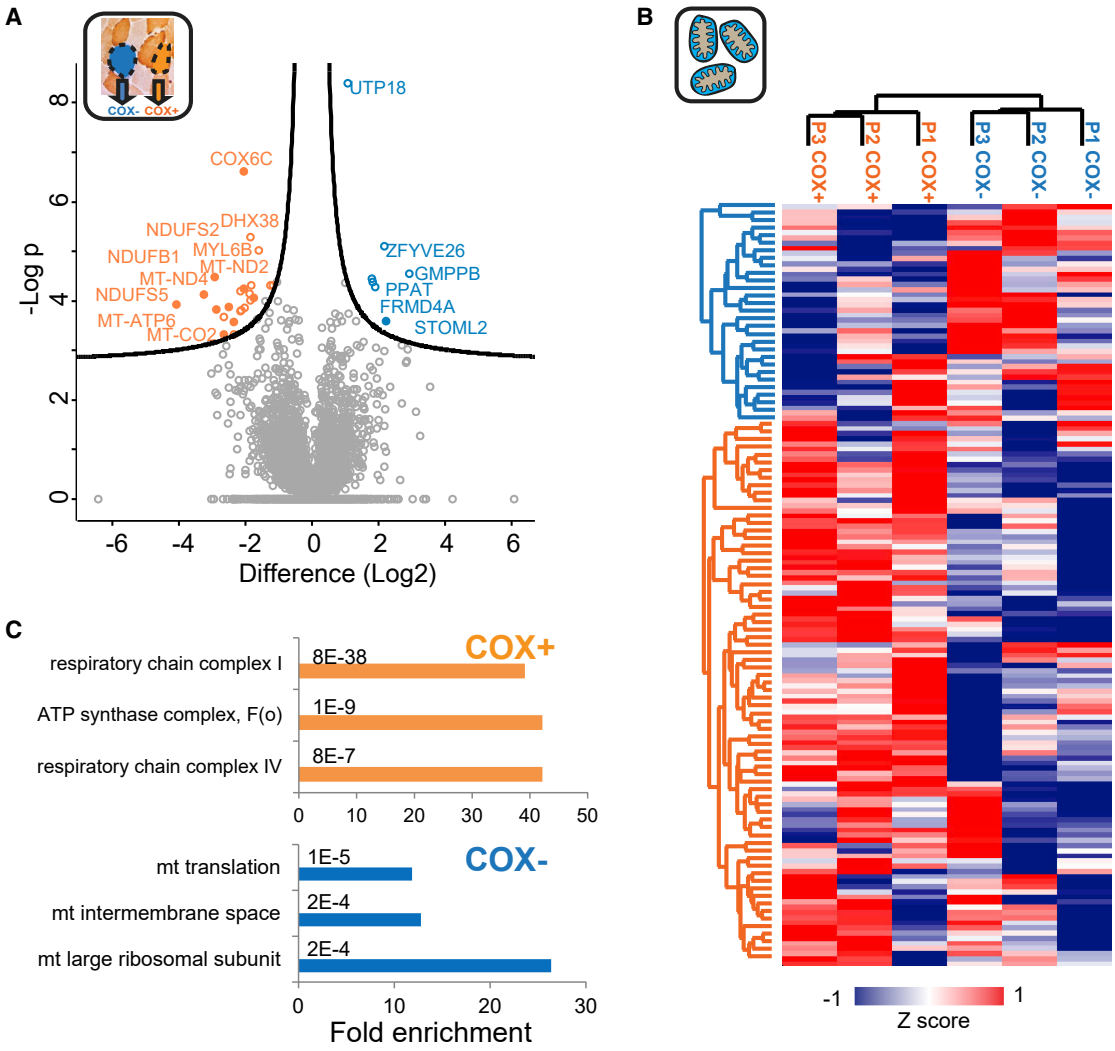

Figure 3. Differences between COX$^+$ and COX$^-$ Muscle Fiber Pools at Whole Proteome and Mitochondrial Proteome Levels

(A) Volcano plot of statistical significance against fold change, showing the most significantly different proteins between COX$^+$ (orange circles) and COX$^-$ fibers (blue circles) in the whole cell proteome. Analysis performed in 5,940 proteins quantified at least once in these samples. Filled circle, mitochondrial proteins.

(B) Hierarchical clusters of mitochondrial proteins (normalized by citrate synthase) with significantly different expression in COX$^+$ and COX$^-$ fiber pools of each patient (labeled P1, P2, P3). Color scale (*Z* scored expression) at the bottom. Each sample is the mean of technical triplicates; missing values were imputed. Cluster separation is shown in color at left.

(C) Bar graphs showing fold increase of the top 3 annotation enrichments of mitochondrial proteins with significantly higher expression in COX$^-$ and COX$^+$ fiber pools (Fisher's exact test, false discovery rate [FDR] 0.02). Test p value is reported on top of each bar.

See also Figure S5 and Tables S7, S8, and S9.

mitochondrial biogenesis based on the literature (Permuth-Wey et al., 2011). Of those, we could quantify 15 proteins in at least 2 samples per group (COX$^-$ versus COX$^+$). Three proteins (transcription termination factor 4, MTERF4; constitutive nitric oxide synthase, NOS1; and the delta subunit of calcium/calmodulin-dependent protein kinase type II, CAMK2D) were significantly higher expressed in COX$^-$ fibers, while 2 proteins (mitogen-activated protein kinase 1, MAPK1; AMP kinase [AMPK] subunit alpha-2, PRKAA2) were significantly higher expressed in COX$^+$ fibers (Table S6). Other critical regulators of mitochondrial biogenesis were, however, not significantly changed (e.g., transcription factor A, mitochondrial [TFAM]) or could not be quantified at all (e.g., peroxisome proliferator-activated receptor gamma co-activator 1alpha [PGC1alpha], CAMK4).

Adaptive Molecular Responses to Mitochondrial Dysfunction at the Cellular Level

The expression of many respiratory chain components was significantly higher in COX$^+$ than in COX$^-$ fibers (volcano plot, Figure 3A). COX$^-$ fibers overexpressed most significantly UTP18, a nucleolar protein involved in ribosomal processing RNA under stress conditions (Yang et al., 2015). The cardiolipin-binding protein STOML2/SLP2 was also upregulated in COX$^-$ fibers (Figure 3A). STOML2 forms a complex with the

fusion-promoting guanosine triphosphatase (GTPase) mitofusin 2 (MFN2) enhancing mitochondrial biogenesis (Christie et al., 2011; Hájek et al., 2007).

We used MitoCarta 2.0 (Calvo et al., 2016) to select the mitochondrial proteins from the dataset (see Bioinformatic and statistical analysis). We normalized mitochondrial protein expression by CS expression. We could thus analyze the proteomes of COX^+ and COX^- fiber pools, correcting for systematic differences of mitochondrial content between patients and sampling differences. t Test comparison showed 148 proteins with significantly different expression between the two groups ($p < 0.05$). Unsupervised hierarchical clustering separated COX^+ and COX^- fibers, revealing enriched GO and keyword terms (Figure 3B; Table S7). COX^+ showed >40-fold enrichments in respiratory chain annotations. COX^- displayed significant enrichments (>25-fold) in mitochondrial ribosomes (Figure 3C). This may be a compensatory mechanism for the defective expression and function of the respiratory chain in COX^- fibers (see Discussion).

Other cell compartments showed a smaller difference between COX^+ and COX^- fibers. We selected the proteins located in the endoplasmic reticulum (ER) using keyword annotations, which yielded 317 proteins that could be quantified in both fiber groups. Fourteen proteins were significantly more expressed in COX^- fibers and 21 in COX^+, among them the ER shaping proteins RTN4 (4.6-fold higher in COX^+, $p < 10^{-5}$) and ATL2 (1.8-fold higher in COX^-, $p < 0.05$). Two proteins induced during ER stress and the unfolded protein response (UPR), SEC63 and ERO1LB, were also significantly higher in COX^- fibers, suggesting a partial activation of this pathway (Figure S5A). The chaperone HSPA5/grp78, a major UPR player, was expressed 1.7-fold higher in COX^- than in COX^+ fibers, although the difference was not significant ($p = 0.06$) (Figure S5A). We also looked at non-blood-related inflammatory markers (GO Biological Process [GOBP] inflammatory response) as readout of muscle damage. Three proteins were expressed at a significantly higher level in COX^+ fibers (IKBKG/NEMO, RPS6KA4, JMJD7) and two in COX^- fibers (APOL2, PLGRKT), indicating no strong activation of this pathway in the fibers of our patient cohort (Figure S5B).

To elucidate the effects of mitochondrial disease on the proteome of individual CPEO patients, we compared the COX^+ and COX^- fibers of each patient. t Test analysis retrieved 182, 34, and 122 proteins with significantly higher expression in the COX^+ fiber pools of patients 1, 2, and 3, respectively (Figure 3; Table S8; STAR Methods). We constructed a Venn diagram highlighting 11 proteins upregulated in all 3 patients and >50-fold enriched in respiratory chain terms (Figure S5C). The same procedure in COX^+ fibers highlighted various annotations of energy metabolism in patients 1 and 3, as well as the enrichment in cysteine oxidation in patient 2. The proteins with significantly higher expression in COX^- fibers amounted to 22, 177, and 92 in the 3 patients, respectively (Figure 3; Table S9; STAR Methods). Only C1QBP/p32 (component 1 Q subcomponent-binding protein) was upregulated in COX^- fibers of all of the patients. C1QBP is a ubiquitous protein of poorly characterized function localized predominantly in the matrix. Approximately 70% of proteins significantly overexpressed in COX^- fibers were specific for 1 patient only. A common feature of patients 1 and 3 was the enrichment in the TCA cycle, possibly an indication of the increased usage of the Krebs cycle to alleviate malfunctioning of the respiratory chain (Figure S5D). Such heterogeneity is likely causing different responses to therapeutic interventions.

Mitochondrial Disease at the Single-Fiber Level

Human slow-type 1 fibers are characterized by oxidative metabolism and more mitochondria than the fast-type 2A and 2X fibers, which have a higher expression of glycolytic enzymes (Murgia et al., 2017). Comparing pure fiber types can thus precisely pinpoint the specific disease pathogenesis at the single-cell level. To this aim, we cut 40 cross-sections of 10-μm thickness from muscle biopsies of 3 patients, histochemically stained every second section as a morphological reference, and excised 20 serial sections of individual fibers using LCM (Figure 1A). With this procedure, each single fiber encompasses 400 μm of tissue. The serial sections of the same fiber were pooled and processed together for MS analysis. We isolated three COX^+ and three COX^- single fibers from each patient. MS-based proteomics allowed us to directly quantify different myosin isoforms and thus determine the fiber type (Table S5) (Murgia et al., 2015). Of 18 single fibers, 13 were pure slow-type 1, as defined by the predominant expression of MYH7, 3 were pure fast fibers expressing a majority (>75%) of MYH2A, and 3 were mixed 1/2A type (Figure 4A). To confirm the precision of fiber type assignment, we selected the proteins involved in contraction (keyword annotation "muscle protein"), which are typically expressed in a fiber type-specific manner. Hierarchical clustering divides the fibers assigned as fast from those assigned as slow. Among the proteins characterizing the two main clusters are myosin and troponin isoforms, specifically segregating into fast and slow gene products (Figure 4B).

Precise fiber type assignment allowed us to focus on the proteome-wide effects of mitochondrial disease in a fiber type-specific manner. We averaged protein expression in all of the slow fibers of each patient, which yielded a separation by PCA of COX^+ and COX^- fibers along component 3, driven by a significant enrichment ($p < 10^{-12}$) in respiratory chain components in COX^+ fibers (Figure 4C). SerpinB3, a major driver of the separation of COX^- slow fibers, is a serine protease inhibitor upregulated by oxidative stress (Ciscato et al., 2014). Combined with a high expression of the nicotinamide nucleotide transhydrogenase (NNT), this indicates that COX^- slow fibers cope with high levels of reactive oxygen species. NNT is expressed more in slow than in fast fibers and is involved in NADPH generation, thus contributing to the buffering of H_2O_2 production (Schiaffino et al., 2015) (Figure 4D).

A t test comparison between the mitochondrial proteomes of COX^+ and COX^- slow fibers yielded 50 significant proteins. As expected, the 22 proteins with higher expression in COX^+ were enriched in oxidative phosphorylation terms ($p < 10^{-10}$). The 28 proteins that were more abundant in COX^- fibers had various intramitochondrial localizations, but formed a highly interconnected network of functional association with two main clusters, as revealed by the STRING database (Szklarczyk et al., 2015) (Figure 4E). One functional cluster highlighted by this analysis is enriched in pyruvate dehydrogenase ($p < 10^{-6}$) and TCA cycle annotations ($p < 10^{-10}$). The other major cluster is enriched

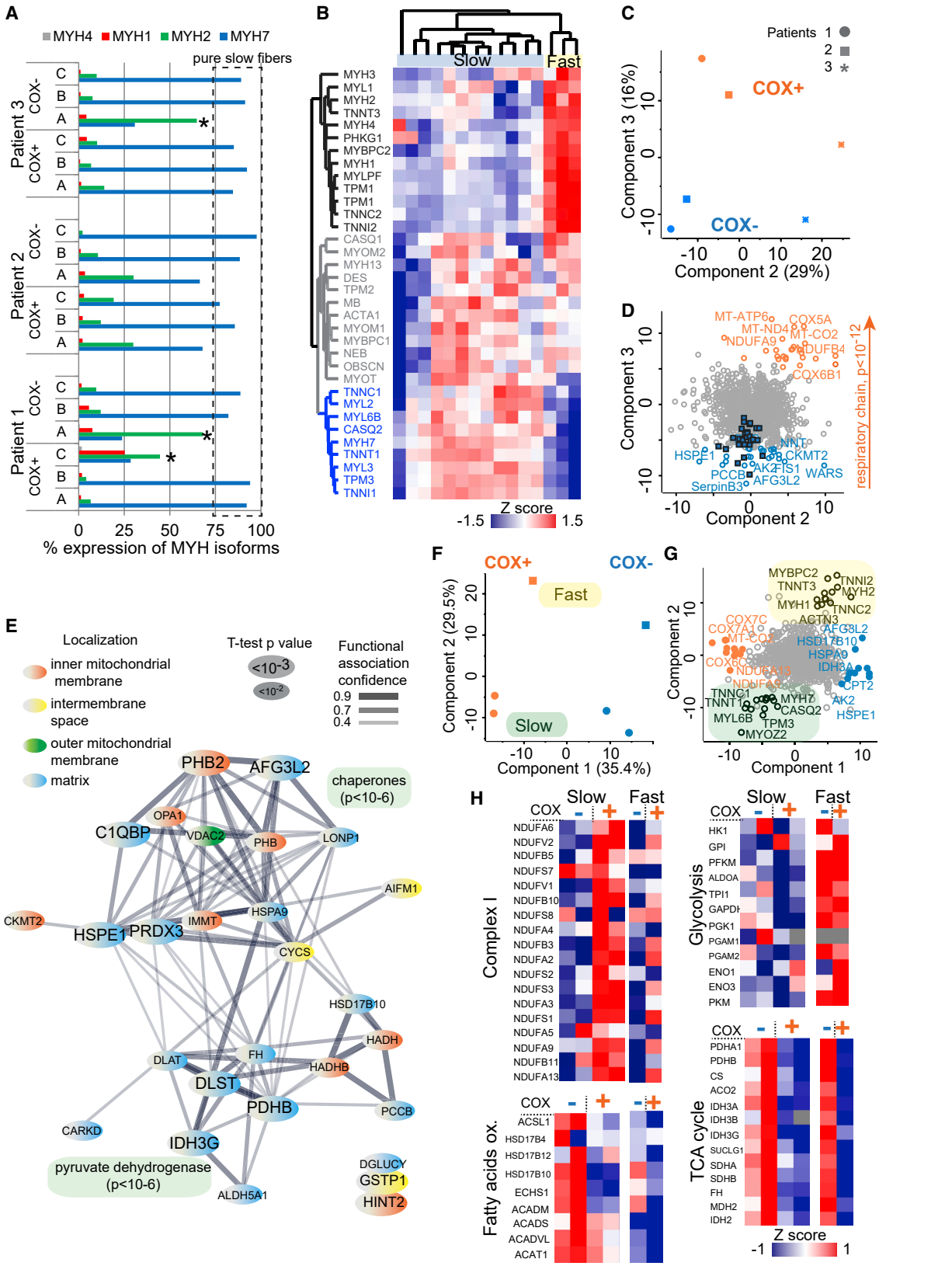

(legend on next page)

in chaperones (GO Molecular Function Unfolded Protein Binding, $p < 10^{-6}$) and includes major players of cristae remodeling, such as OPA1, the MICOS complex subunit IMMT, the scaffolding proteins PHB and PHB2, and proteases such as LONP1 and AFG3L2, important for quality control, which were all >1.8-fold higher in COX^- fibers (Table S10) (Baker et al., 2019). We extended this analysis by curating a list of 30 proteins involved in mitochondrial dynamics and cristae remodeling and quantifying their expression in COX^- and COX^+ fiber pools. Twelve proteins had >1.5-fold higher expression in COX^- than in COX^+ fibers, whereas only 2 were >1.5 higher in COX^+ fibers. Among the latter is DNM1L/DRP1, a master regulator of fission. In addition to the protease AFG3L2 and the MICOS complex protein IMMT, the protease YME1L1 was significantly higher in COX^- fiber pools ($p < 0.001$) (Table S11).

Finally, we compared the effects of mitochondrial disease at the proteome level in single slow and fast fibers from the same patient. The 4 slow fibers and 2 fast fibers obtained from patient 1 (see Figure 4A) could be separated by principal-component analysis (PCA) along component 1 into COX^+ and COX^- groups. Furthermore, slow and fast fibers were clearly distinguished along component 2, driven by key determinants of fiber types such as myosin and troponin isoforms (Figures 4F and 4G). We then directly compared the expression of individual metabolic pathways in the 4 slow and 2 fast fibers from patient 1. Both COX^+ slow fibers had a higher expression of the respiratory chain complex I than the corresponding COX^- fibers. This difference could be observed at generally lower expression levels also in the two fast fibers, which contain fewer mitochondria than slow fibers (Figure 4H). By measuring the expression of respiratory chain components in COX^+ and COX^- single fibers of the same patient, here, we quantify the net effect of disease on mitochondrial protein expression in a fiber type-specific manner, devoid of variability among individuals. Regulated proteins were indeed different between slow and fast fibers of the same individual. Measuring the COX^+:COX^- expression ratio, we observed 62% similarity between the fast and slow fibers of patient 1. Conversely, 38% of the measured proteome was differently regulated in the 2 fiber types (21% higher in fast, 17% higher in slow) (Figure S6). Glycolytic enzymes were higher in fast fibers independent of COX status, indicating that the upregulation of glycolysis is not a common compensation mechanism for energy deficit in COX^- fibers. Conversely, TCA cycle enzymes were similarly overexpressed in COX^- fibers, regardless of fiber type. This pathway is likely a fiber type-independent compensatory mechanism for the respiratory chain deficiency in the patient. We then focused on fatty acids beta-oxidation, confirming that this pathway has higher expression in the mitochondria of slow fibers than in those of fast fibers (Murgia et al., 2015). Bioenergetic deficiency in COX^- slow fibers was associated with the further upregulation of fatty acid oxidation enzymes, which was essentially negligible in fast fibers (Figure 4H).

DISCUSSION

Mitochondrial disorders, in a strict sense, are the consequence of mutations affecting the respiratory chain. They frequently hit skeletal muscle, while other tissues are involved in a disease-specific manner. The overall relation between mtDNA mutations and clinical presentation is complex and poorly characterized at the molecular level. A diagnostic marker is the appearance of RRFs reflecting metabolic decompensation above a certain threshold of mutant mtDNA (heteroplasmy). Deeper insight into the underlying molecular mechanisms is needed to better understand the pathogenesis of mitochondrial disorders. To provide mechanistic details, this analysis needs a combination of fine tissue dissection and large-scale technologies.

Our workflow allowed the quantification of >2,000 proteins from minute amounts of patient material in just 2 h of measurement time. We could clearly show significantly higher expression of respiratory chain components in COX^+ than in COX^- fibers. Conversely, assembly factors of complexes I–IV were higher in COX^- fibers as compared to COX^+ fibers, some of them statistically significant (Figure S4), which may indicate a compensatory mechanism. The difference in the expression of mitochondrial biogenesis factors was surprisingly small between COX^- and

Figure 4. Single Fiber Features and Fiber Type Specificity in Mitochondrial Myopathies

(A) Expression of 4 adult isoforms of myosin heavy chain (MYH) in 6 individual fibers (labeled A, B, and C for both COX^- and COX^+) of each patient. The summed intensities of MYH7 (characterizing type 1/slow fibers), MYH2 (characterizing type 2A/fast fibers), MYH1 (characterizing type 2X/fast fibers), and type 2B (characterizing rodent type 2B/fast fibers and only present in trace amounts in humans) were used as 100%. Fibers with >75% of MYH7 were considered pure type 1/slow fibers. Fast fibers are marked by an asterisk.

(B) Hierarchical clustering of proteins involved in muscle contraction, showing cluster segregation of fast and slow specific isoforms.

(C) Principal-component analysis (PCA) of mitochondrial proteins of pure slow single fibers. Fibers from 3 patients (average of all slow fibers of each individual) segregate into COX^+ (orange) and COX^- (blue) along component 2.

(D) Loadings of the PCA showing major drivers of separation and significant enrichments (arrow and corresponding p value). Mitochondrial proteins with significantly higher expression in COX^- fibers are marked with a black line.

(E) Functional interaction network analysis of proteins with significantly higher expression in COX^- slow fibers. Fibers are color-coded based on intra-mitochondrial localization; box size reflects p value in the COX^+ versus COX^- t test and line thickness marks the functional interaction confidence as defined in the STRING database. Proteins significantly overexpressed in COX^- fibers but without known functional interactions with the rest of the network are shown at bottom right. Annotation enrichments with p value are marked in the green areas.

(F) PCA of all single fibers isolated from patient 1. Dots mark slow fibers and squares mark fast fibers, based on the MYH quantifications shown in (A).

(G) PCA loadings showing drivers of the segregation into component 1 (separating COX^+ and COX^- fibers) and component 2 (separating fibers based on fiber type). The yellow area highlights fast fiber type-specific proteins, such as fast troponins. The corresponding slow isoforms are highlighted in green.

(H) Heatmap of normalized protein expression (*Z* scored, scale at bottom) in single fibers from 1 patient, 4 slow fibers in total (2 COX^+ and 2 COX^-, as indicated) and 2 fast fibers, 1 COX^- and 1 COX^+, respectively. Only proteins expressed in all of the fibers were used for the analysis. Respiratory chain complex I, glycolysis, TCA cycle, and fatty acid oxidation are shown. Gray squares, not quantified.

See also Figures S5 and S6 and Tables S5, S10, and S11.

COX^+ fibers (Table S6). This is in contrast to light and electron microscopy, in which signs of increased biogenesis (RRFs) are more frequent and more marked in COX^- than in COX^+ fibers (DiMauro and Schon, 2003).

Our results show that COX^+ and COX^- fibers are significantly different at the proteome level. COX^- fibers upregulated mitochondrial ribosomes and proteins involved in the control of translation (Figure 3). Among these, C1QBP, upregulated in the COX^- fibers of all of the patients (Figure S4), is required for functional mitoribosome formation and protein synthesis (Yagi et al., 2012). Mutations in C1QBP were described in patients with mitochondrial cardiomyopathy and combined respiratory chain enzyme deficiency (Feichtinger et al., 2017).

COX^- fibers also upregulate mitochondrial chaperones and STOML2 (Figure 3). The latter organizes cardiolipin-enriched microdomains in the inner membrane and controls the assembly of functional respiratory supercomplexes (Mitsopoulos et al., 2015). We measured a significant increase of several members of the OPA1-dependent cristae remodeling program in COX^- single slow fibers, suggesting that they may be producing more cristae. Ultrastructural analyses of patients with CPEO and other mitochondrial disorders show several morphological abnormalities, such as extended "onion-like" concentric cristae and "donut mitochondria," indicating elongation and hyperbranching (Bacalhau et al., 2018; Vincent et al., 2016). Because the ultimate effects of mtDNA mutations will reflect on the fiber metabolic profile, it would be interesting to carry out a metabolomic analysis of COX^+ and COX^- fibers following the technological progress of this field.

A novelty of our proteomic approach is the ability to analyze mitochondrial disease in individual fibers, by following and cutting the same fiber across 20 serial sections. Skeletal muscle has a heterogeneous composition in slow type 1 and fast type 2 fibers, with different mitochondrial content. In the context of mitochondrial disorders, fiber type composition is superimposed onto the pathological process giving rise to the COX^+ and COX^- fiber mosaic. To reduce the variables causing this extreme heterogeneity, we selected a pool of single fibers that were type 1 slow based on the expression of MYH7, the slow myosin heavy-chain isoform (Figure 4). We thus eliminated the confounding effects of the heterogeneous fiber type composition, revealing a coordinated increase of a network of functionally interacting proteins involved in mitochondrial dynamics and quality control. We found that eight of these proteins were expressed at a significantly higher level in COX^- than in COX^+ slow fibers. We observed a significant upregulation of the OPA1-dependent cristae remodeling program in COX^- slow fibers. This pathway controls the tightening of mitochondrial cristae, which results in higher respiratory efficiency and limits the production of reactive oxygen species and cytochrome *c* release (Varanita et al., 2015). Comparing fibers from the same patient, we showed that the upregulation of TCA cycle enzymes occurs in both fast and slow COX^- fibers and likely represents a fiber type-independent compensatory mechanism for the energy deficit caused by disease. Only COX^- slow fibers, however, upregulated the enzymes involved in fatty acids beta-oxidation. Our single fiber analysis has thus uncovered a fiber type-specific metabolic shift induced by mitochondrial disease.

It remains to be determined whether the combination of the observed compensatory mechanisms ultimately provides a relief from the energy imbalance caused by respiratory chain defect or whether it contributes to the pathogenesis of the disease by causing proteotoxic stress and mitochondrial integrated stress response. It will also be of interest to assess the role of FGF21, a recently characterized mediator of mitochondrial stress responses, in the proteomic rearrangements that we have measured in COX^- fibers (Forsström et al., 2019). Predicting the outcome of adaptive responses in mitochondria has traditionally proven extremely complex. In contrast to CPEO and most related disorders, in which RRFs are mostly COX^-, muscle from MELAS patients shows predominantly COX^+ RRFs. The fact that respiratory activity was more severely compromised in MELAS than in CPEO patients by ^{31}P magnetic resonance (MR) spectroscopy in one study (Liu et al., 2014) led to the hypothesis that increased COX expression may worsen the phenotype by impinging on the catabolism of nitric oxide (Balke et al., 2019). This hypothesis, however, did not take into account the predominant complex I defect in MELAS. In CPEO, it is clear that higher proportions of mtDNA deletion lead to higher numbers of COX^- fibers and to less bioenergetic activity (Gellerich et al., 2002).

In conclusion, metabolic decompensation in COX^- fibers is accompanied by an extensive rearrangement of the mitochondrial proteome. This involves the upregulation of metabolic pathways possibly serving as compensatory mechanisms for the bioenergetic deficit causing the disease, as well as of chaperones, reactive oxygen species (ROS) scavengers, and proteins that control inner membrane architecture and supercomplex formation. Further technological developments leading to a systems view of mitochondrial proteome remodeling at the muscle fiber level will be instrumental for the development of targeted therapies for mitochondrial disorders.

STAR★METHODS

Detailed methods are provided in the online version of this paper and include the following:

- KEY RESOURCES TABLE
- LEAD CONTACT AND MATERIALS AVAILABILITY
- EXPERIMENTAL MODEL AND SUBJECT DETAILS
  - Patients, study design and approvals
  - Cell culture
- METHOD DETAILS
  - Tissue preparation for cryosectioning
  - Sequential cytochrome *c* oxidase / succinate dehydrogenase (COX/SDH) histochemistry
  - Laser capture microdissection (LCM)
  - Peptide preparation from muscle fiber sections, total muscle lysate and myoblasts
  - High pH reversed-phase fractionation
  - Liquid Chromatography Tandem Mass Spectrometry (LC-MS/MS) analysis
- QUANTIFICATION AND STATISTICAL ANALYSIS
  - Computational proteomics
  - Bioinformatic and statistical analysis

SUPPLEMENTAL INFORMATION

Supplemental Information can be found online at https://doi.org/10.1016/j.celrep.2019.11.055.

ACKNOWLEDGMENTS

We acknowledge all of the members of the Department of Proteomics and Signal Transduction; N. Nagaraj and S. Schiaffino for help and fruitful discussions; C. Deiml, I. Paron, M. Wiessner, and I. Brandstetter for technical assistance; and C. Laub for help with LCM. We acknowledge the PRIDE Team for the data deposition. This work was supported by the Max Planck Society for the Advancement of Science; the Louis Jeantet Foundation; the German Bundesministerium für Bildung und Forschung (BMBF) through the project mitoNET (01GM1906A) and E-Rare project GENOMIT (01GM1603); and by the European Union's Horizon 2020 research and innovation program under grant agreement 686547 (MSmed project).

AUTHOR CONTRIBUTIONS

Conceptualization and Methodology, T.K., M. Mann, and M. Murgia; Investigation, M. Murgia, J.T., P.E.G., and S.D.; Validation, M. Murgia and J.T; Resources, T.K. and M. Mann; Formal Analysis, M. Murgia, M. Mann, and T.K.; Writing, M. Murgia, M. Mann and T.K.; Funding Acquisition, M. Mann and T.K. All of the authors participated in the discussion and revision of the manuscript. All of the authors read and approved the final manuscript.

DECLARATION OF INTERESTS

The authors declare no competing interests.

Received: May 7, 2019
Revised: September 30, 2019
Accepted: November 13, 2019
Published: December 17, 2019

REFERENCES

Alston, C.L., Rocha, M.C., Lax, N.Z., Turnbull, D.M., and Taylor, R.W. (2017). The genetics and pathology of mitochondrial disease. J. Pathol. *241*, 236–250.

Bacalhau, M., Simões, M., Rocha, M.C., Hardy, S.A., Vincent, A.E., Durães, J., Macário, M.C., Santos, M.J., Rebelo, O., Lopes, C., et al. (2018). Disclosing the functional changes of two genetic alterations in a patient with Chronic Progressive External Ophthalmoplegia: Report of the novel mtDNA m.7486G>A variant. Neuromuscul. Disord. *28*, 350–360.

Baker, N., Patel, J., and Khacho, M. (2019). Linking mitochondrial dynamics, cristae remodeling and supercomplex formation: How mitochondrial structure can regulate bioenergetics. Mitochondrion, S1567-7249(19)30024-8.

Balke, J.E., Zhang, L., and Percival, J.M. (2019). Neuronal nitric oxide synthase (nNOS) splice variant function: Insights into nitric oxide signaling from skeletal muscle. Nitric Oxide *82*, 35–47.

Calvo, S.E., Clauser, K.R., and Mootha, V.K. (2016). MitoCarta2.0: an updated inventory of mammalian mitochondrial proteins. Nucleic Acids Res. *44* (*D1*), D1251–D1257.

Christie, D.A., Lemke, C.D., Elias, I.M., Chau, L.A., Kirchhof, M.G., Li, B., Ball, E.H., Dunn, S.D., Hatch, G.M., and Madrenas, J. (2011). Stomatin-like protein 2 binds cardiolipin and regulates mitochondrial biogenesis and function. Mol. Cell. Biol. *31*, 3845–3856.

Ciscato, F., Sciacovelli, M., Villano, G., Turato, C., Bernardi, P., Rasola, A., and Pontisso, P. (2014). SERPINB3 protects from oxidative damage by chemotherapeutics through inhibition of mitochondrial respiratory complex I. Oncotarget *5*, 2418–2427.

Cox, J., and Mann, M. (2008). MaxQuant enables high peptide identification rates, individualized p.p.b.-range mass accuracies and proteome-wide protein quantification. Nat. Biotechnol. *26*, 1367–1372.

Cox, J., Neuhauser, N., Michalski, A., Scheltema, R.A., Olsen, J.V., and Mann, M. (2011). Andromeda: a peptide search engine integrated into the MaxQuant environment. J. Proteome Res. *10*, 1794–1805.

Cox, J., Hein, M.Y., Luber, C.A., Paron, I., Nagaraj, N., and Mann, M. (2014). Accurate proteome-wide label-free quantification by delayed normalization and maximal peptide ratio extraction, termed MaxLFQ. Mol. Cell. Proteomics *13*, 2513–2526.

Deshmukh, A.S., Murgia, M., Nagaraj, N., Treebak, J.T., Cox, J., and Mann, M. (2015). Deep proteomics of mouse skeletal muscle enables quantitation of protein isoforms, metabolic pathways, and transcription factors. Mol. Cell. Proteomics *14*, 841–853.

DiMauro, S., and Schon, E.A. (2003). Mitochondrial respiratory-chain diseases. N. Engl. J. Med. *348*, 2656–2668.

Feichtinger, R.G., Oláhová, M., Kishita, Y., Garone, C., Kremer, L.S., Yagi, M., Uchiumi, T., Jourdain, A.A., Thompson, K., D'Souza, A.R., et al. (2017). Biallelic C1QBP Mutations Cause Severe Neonatal-, Childhood-, or Later-Onset Cardiomyopathy Associated with Combined Respiratory-Chain Deficiencies. Am. J. Hum. Genet. *101*, 525–538.

Feldkirchner, S., Walter, M.C., Müller, S., Kubny, C., Krause, S., Kress, W., Hanisch, F.G., Schoser, B., and Schessl, J. (2013). Proteomic characterization of aggregate components in an intrafamilial variable FHL1-associated myopathy. Neuromuscul. Disord. *23*, 418–426.

Forsström, S., Jackson, C.B., Carroll, C.J., Kuronen, M., Pirinen, E., Pradhan, S., Marmyleva, A., Auranen, M., Kleine, I.M., Khan, N.A., et al. (2019). Fibroblast Growth Factor 21 Drives Dynamics of Local and Systemic Stress Responses in Mitochondrial Myopathy with mtDNA Deletions. Cell Metab. *Sep 9*, S1550-4131(19)30448-6.

Gellerich, F.N., Deschauer, M., Chen, Y., Müller, T., Neudecker, S., and Zierz, S. (2002). Mitochondrial respiratory rates and activities of respiratory chain complexes correlate linearly with heteroplasmy of deleted mtDNA without threshold and independently of deletion size. Biochim. Biophys. Acta *1556*, 41–52.

Gorman, G.S., Schaefer, A.M., Ng, Y., Gomez, N., Blakely, E.L., Alston, C.L., Feeney, C., Horvath, R., Yu-Wai-Man, P., Chinnery, P.F., et al. (2015). Prevalence of nuclear and mitochondrial DNA mutations related to adult mitochondrial disease. Ann. Neurol. *77*, 753–759.

Greaves, L.C., Yu-Wai-Man, P., Blakely, E.L., Krishnan, K.J., Beadle, N.E., Kerin, J., Barron, M.J., Griffiths, P.G., Dickinson, A.J., Turnbull, D.M., and Taylor, R.W. (2010). Mitochondrial DNA defects and selective extraocular muscle involvement in CPEO. Invest. Ophthalmol. Vis. Sci. *51*, 3340–3346.

Hájek, P., Chomyn, A., and Attardi, G. (2007). Identification of a novel mitochondrial complex containing mitofusin 2 and stomatin-like protein 2. J. Biol. Chem. *282*, 5670–5681.

Jiao, X., Sherman, B.T., Huang da, W., Stephens, R., Baseler, M.W., Lane, H.C., and Lempicki, R.A. (2012). DAVID-WS: a stateful web service to facilitate gene/protein list analysis. Bioinformatics *28*, 1805–1806.

Kley, R.A., Maerkens, A., Leber, Y., Theis, V., Schreiner, A., van der Ven, P.F., Uszkoreit, J., Stephan, C., Eulitz, S., Euler, N., et al. (2013). A combined laser microdissection and mass spectrometry approach reveals new disease relevant proteins accumulating in aggregates of filaminopathy patients. Mol. Cell. Proteomics *12*, 215–227.

Koob, A.O., Bruns, L., Prassler, C., Masliah, E., Klopstock, T., and Bender, A. (2012). Protein analysis through Western blot of cells excised individually from human brain and muscle tissue. Anal. Biochem. *425*, 120–124.

Kulak, N.A., Pichler, G., Paron, I., Nagaraj, N., and Mann, M. (2014). Minimal, encapsulated proteomic-sample processing applied to copy-number estimation in eukaryotic cells. Nat. Methods *11*, 319–324.

Kulak, N.A., Geyer, P.E., and Mann, M. (2017). Loss-less Nano-fractionator for High Sensitivity, High Coverage Proteomics. Mol. Cell. Proteomics *16*, 694–705.

Lightowlers, R.N., Taylor, R.W., and Turnbull, D.M. (2015). Mutations causing mitochondrial disease: What is new and what challenges remain? Science *349*, 1494–1499.

Liu, A.H., Niu, F.N., Chang, L.L., Zhang, B., Liu, Z., Chen, J.Y., Zhou, Q., Wu, H.Y., and Xu, Y. (2014). High cytochrome c oxidase expression links to severe skeletal energy failure by (31)P-MRS spectroscopy in mitochondrial encephalomyopathy, lactic acidosis, and stroke-like episodes. CNS Neurosci. Ther. *20*, 509–514.

Maerkens, A., Kley, R.A., Olivé, M., Theis, V., van der Ven, P.F., Reimann, J., Milting, H., Schreiner, A., Uszkoreit, J., Eisenacher, M., et al. (2013). Differential proteomic analysis of abnormal intramyoplasmic aggregates in desminopathy. J. Proteomics *90*, 14–27.

Mitsopoulos, P., Chang, Y.H., Wai, T., König, T., Dunn, S.D., Langer, T., and Madrenas, J. (2015). Stomatin-like protein 2 is required for in vivo mitochondrial respiratory chain supercomplex formation and optimal cell function. Mol. Cell. Biol. *35*, 1838–1847.

Murgia, M., Nagaraj, N., Deshmukh, A.S., Zeiler, M., Cancellara, P., Moretti, I., Reggiani, C., Schiaffino, S., and Mann, M. (2015). Single muscle fiber proteomics reveals unexpected mitochondrial specialization. EMBO Rep. *16*, 387–395.

Murgia, M., Toniolo, L., Nagaraj, N., Ciciliot, S., Vindigni, V., Schiaffino, S., Reggiani, C., and Mann, M. (2017). Single Muscle Fiber Proteomics Reveals Fiber-Type-Specific Features of Human Muscle Aging. Cell Rep. *19*, 2396–2409.

Old, S.L., and Johnson, M.A. (1989). Methods of microphotometric assay of succinate dehydrogenase and cytochrome c oxidase activities for use on human skeletal muscle. Histochem. J. *21*, 545–555.

Permuth-Wey, J., Chen, Y.A., Tsai, Y.Y., Chen, Z., Qu, X., Lancaster, J.M., Stockwell, H., Dagne, G., Iversen, E., Risch, H., et al. (2011). Inherited variants in mitochondrial biogenesis genes may influence epithelial ovarian cancer risk. Cancer Epidemiol. Biomarkers Prev. *20*, 1131–1145.

Schiaffino, S., Reggiani, C., Kostrominova, T.Y., Mann, M., and Murgia, M. (2015). Mitochondrial specialization revealed by single muscle fiber proteomics: focus on the Krebs cycle. Scand. J. Med. Sci. Sports *25* (*Suppl 4*), 41–48.

Schon, E.A., DiMauro, S., and Hirano, M. (2012). Human mitochondrial DNA: roles of inherited and somatic mutations. Nat. Rev. Genet. *13*, 878–890.

Spinazzola, A., and Zeviani, M. (2009). Mitochondrial diseases: a cross-talk between mitochondrial and nuclear genomes. Adv. Exp. Med. Biol. *652*, 69–84.

Szklarczyk, D., Franceschini, A., Wyder, S., Forslund, K., Heller, D., Huerta-Cepas, J., Simonovic, M., Roth, A., Santos, A., Tsafou, K.P., et al. (2015). STRING v10: protein-protein interaction networks, integrated over the tree of life. Nucleic Acids Res. *43*, D447–D452.

Tyanova, S., Temu, T., and Cox, J. (2016a). The MaxQuant computational platform for mass spectrometry-based shotgun proteomics. Nat. Protoc. *11*, 2301–2319.

Tyanova, S., Temu, T., Sinitcyn, P., Carlson, A., Hein, M.Y., Geiger, T., Mann, M., and Cox, J. (2016b). The Perseus computational platform for comprehensive analysis of (prote)omics data. Nat. Methods *13*, 731–740.

Varanita, T., Soriano, M.E., Romanello, V., Zaglia, T., Quintana-Cabrera, R., Semenzato, M., Menabò, R., Costa, V., Civiletto, G., Pesce, P., et al. (2015). The OPA1-dependent mitochondrial cristae remodeling pathway controls atrophic, apoptotic, and ischemic tissue damage. Cell Metab. *21*, 834–844.

Vincent, A.E., Ng, Y.S., White, K., Davey, T., Mannella, C., Falkous, G., Feeney, C., Schaefer, A.M., McFarland, R., Gorman, G.S., et al. (2016). The Spectrum of Mitochondrial Ultrastructural Defects in Mitochondrial Myopathy. Sci. Rep. *6*, 30610.

Yagi, M., Uchiumi, T., Takazaki, S., Okuno, B., Nomura, M., Yoshida, S., Kanki, T., and Kang, D. (2012). p32/gC1qR is indispensable for fetal development and mitochondrial translation: importance of its RNA-binding ability. Nucleic Acids Res. *40*, 9717–9737.

Yang, H.W., Kim, T.M., Song, S.S., Menon, L., Jiang, X., Huang, W., Black, P.M., Park, P.J., Carroll, R.S., and Johnson, M.D. (2015). A small subunit processome protein promotes cancer by altering translation. Oncogene *34*, 4471–4481.

STAR★METHODS

KEY RESOURCES TABLE

REAGENT or RESOURCE	SOURCE	IDENTIFIER
Biological Samples		
Cultured human myoblasts	mitoNET Biobank	http://mitonet.org
Muscle biopsies	mitoNET Biobank	http://mitonet.org
Chemicals, Peptides, and Recombinant Proteins		
Cytochrome *c* (equine recombinant, expressed in *E. coli*)	Sigma	Cat# C-2506
Diaminobenzidine tetrahydrochloride	Sigma	Cat# D-5637
Sodium succinate	Sigma	Cat# S-2378
Sodium azide	Sigma	Cat# BDH30111
Nitroblue tetrazolium	Sigma	Cat# N6876
Eukitt	Sigma	Cat# 03989
Catalase	Sigma	Cat# C-9322
PBS (0.2M, Ph7.5)	Sigma	Cat# P0014
PBS (0.1M, Ph7.4)	Sigma	Cat# P0008
Phenazine methosulphate	Sigma	Cat# P9625
Chloracetamide	Sigma	Cat# C0267
Trypsin	Sigma	Cat# T6567
Lysyl Endopeptidase (Lys-C)	Wako Chemicals	Cat# 125-05061
Sodium deoxycholate	Thermo Fischer Scientific	Cat# 89904
TCEP (tris(2-carboxyethyl)phosphine)	Thermo Fischer Scientific	Cat# PG82090
Acetonitrile	Thermo Fischer Scientific	Cat# 100029
Ammonia	Thermo Fischer Scientific	Cat# 533003
Formic acid	Thermo Fischer Scientific	Cat# 533002
Deposited Data		
Proteomic dataset with raw and processed data	This paper	ProteomeXchange PXD010489
Software and Algorithms		
MaxQuant	Cox and Mann, 2008	https://www.maxquant.org/
Perseus	Tyanova et al., 2016b	https://maxquant.org/perseus/
Other		
Laser capture microdissection system	Leica	LMD 7000
Loss-less Nano-fractionator	PreOmics, Kulak et al., 2017	Spider fractionator
Leica Membrane Slides © PEN membrane 2.0 μm	Micro Dissect Gmbh (Herborn)	Cat# 11505158
Slides superfrost	Menzel GmbH	Cat# 7201277
Coverslips	IDL (Nidderau)	Cat# 190002450
0.5ml Laser capture microdissection -Tube	Thermo Fischer Scientific	Cat# AB-0350
FastPrep®-24 homogenizer	MP Biomedicals	https://eu.mpbio.com/fastprep-24-5g-instrument
Bioruptor	Diagenode	https://www.diagenode.com/en
Nanodrop 2000 Spectrophotometer	Thermo Fischer Scientific	https://www.thermofisher.com/us/en/home.html

LEAD CONTACT AND MATERIALS AVAILABILITY

Further information and requests for resources should be directed to and will be fulfilled by the Lead Contact, Thomas Klopstock (tklopsto@med.lmu.de). This study did not generate new unique reagents.

EXPERIMENTAL MODEL AND SUBJECT DETAILS

Patients, study design and approvals

All of the muscle specimens and myoblast cells were obtained from the biobank of the German network for mitochondrial disorders (mitoNET) at the Friedrich-Baur-Institute. The research project was approved by the Ethics Committee of the LMU Munich (N. 198-15) and the study has been performed in accordance with the ethical standards laid down in the 1964 Declaration of Helsinki. Muscle biopsies had been obtained for diagnostic purposes and written informed consent had been obtained from the patients. For the study, we randomly selected 3 patients with CPEO, defined by the pathognomonic clinical phenotype, the presence of RRF on muscle biopsy and detection of a mtDNA deletion (Table S4). All patients were of European origin, two males (age 38 and 49) and one female (age 32). Diagnostic specimens had been collected from the right deltoid or left quadriceps muscle by open biopsy, frozen in liquid nitrogen and stored at −80°C. The control myoblast cells used for the library were randomly selected from 3 patients with no known mitochondrial disorder.

Cell culture

Primary cell lines of human myoblasts used for the peptide library were isolated from muscle biopsies of individuals without known mitochondrial disease and grown in DMEM supplemented with penicillin/streptomycin, L-glutamine, and 10% FBS. A pool of three cell lines (from male and female patients) was used for the peptide preparation.

METHOD DETAILS

Tissue preparation for cryosectioning

Muscle specimens were transferred in liquid nitrogen to the cryostat. Alternate serial sections (10 μm) were adhered to Superfrost plus microscope slides for histochemical staining and to membrane slides for laser microdissection. Superfrost plus slides were air-dried for about 24h and then stored at −20°C for the next histochemical staining. The membrane slides were stored at −80°C prior to cutting and processing for MS-based proteomics.

Sequential cytochrome *c* oxidase / succinate dehydrogenase (COX/SDH) histochemistry

Slides were allowed to dry at room temperature for 10 min and processed according to standard protocol (Old and Johnson, 1989). For COX staining, sections were incubated in COX medium (100 μM cytochrome *c*, 4 mM diaminobenzidine tetrahydrochloride, and 20 μg/ml catalase in 0.2 M phosphate buffer, pH 7.0) for 90 min at 37°C. Sections were then washed in standard PBS, pH 7.4 (2 × 5 min) and incubated in SDH medium (130 mM sodium succinate, 200 μM phenazine methosulphate, 1 mM sodium azide, 1.5 mM nitroblue tetrazolium in 0.2 M phosphate buffer, pH 7.0) for 120 min at 37°C. Sections were then washed in PBS, pH 7.4 (2 × 5 min), rinsed in distilled water and dehydrated in an increasing ethanol series up to 100%, prior to incubation in xylene and mounting in Eukitt.

Laser capture microdissection (LCM)

The procedure was carried out essentially as we described previously (Koob et al., 2012). The images of whole COX/SDH-stained slides and sections of interest were acquired and stored using a Leica LMD 7000 System. Next, we observed the unstained serial sections under the microscope at various magnifications and compared with the pictures of stained sections individually. According to the recognizable histochemical features of COX+ and COX- cells, we determined the coordinates of their corresponding unstained cells and dissected them by LCM. 100 COX+ and 100 COX- cells were dissected for each patient. Similarly, we selected 3 COX+ and 3 COX- single fibers with clearly recognizable histochemical features for each patient, then excised 20 COX+ or 20 COX- serial sections for each fiber separately. The whole procedure was precisely timed for each sample and carried out in less than 30 min at room temperature. Fiber sections were captured by cutting the region of interest onto the caps of 0.5ml Thermo-Tube, which were carefully closed and immediately frozen in liquid nitrogen at the end of the procedure. Samples were stored at −80°C until used. Protein amount was determined in serial dilutions of fiber section pools resuspended in 8 M urea containing 10 mM Tris-HCl, pH 8.5, measuring the fluorescence emission of tryptophan (excitation 280 nm, emission 350 nm).

Peptide preparation from muscle fiber sections, total muscle lysate and myoblasts

Fiber sections were resuspended in 10 μl of sodium deoxycholate (SDC)-based reduction and alkylation buffer by extensively washing the collection tube after laser capture. Total muscle (60 mg) was crushed in liquid nitrogen using a mortar and pestle. Powdered muscle samples and myoblast cells (3x 10^6 cells) were resuspended in 310 μl (5 μl/mg) and 200 μl SDC buffer, respectively. The total muscle sample was further mixed (six times 30 s and cooled on ice in between) using a FastPrep®-24 Instrument (MP Biomedicals). Samples were further boiled for 10 min to denature proteins (Kulak et al., 2014).

For total muscle and myoblast lysate (not for sections), protein concentration was measured using the Tryptophan assay. The muscle sections (entire sample) were digested with 0.5 μg of trypsin and 0.5 μg of LysC per sample at 37°C, under continuous stirring. For total muscle lysate and myoblasts, 250 μg were digested overnight with Lys-C and trypsin in a 1:25 ratio (μg of enzyme to μg of protein) at 37°C, under continuous stirring. On the following day, samples were sonicated using a Bioruptor (Diagenode, 15 cycles of

30 s) and further digested for 3 h with Lys-C and trypsin (1:100 ratio). Peptides were acidified to a final concentration of 0.1% trifluoroacetic acid (TFA) for SDB-RPS binding and 40 μg of peptides were loaded on four 14-gauge Stage-Tip plugs. Peptides were washed first with wash buffers (P.O. 00001, PreOmics GmbH) using an in house made Stage-Tip centrifuge at 2000 x g. Peptides were eluted with 60 μl of elution buffer (80% acetonitrile / 1% ammonia) into auto sampler vials and dried using a SpeedVac centrifuge (Eppendorf, Concentrator plus). Peptides were resuspended in 2% acetonitrile / 0.1% TFA before peptide concentration estimation using a Nanodrop spectrophotometer (Thermo Fischer Scientific). Purified peptides from total muscle and myoblast lysates were further subjected to fractionation.

High pH reversed-phase fractionation

We applied a pre-fractionation based on a high pH buffer system and resulting in an orthogonal separation to the online LC that is directly coupled to the MS. High pH reversed-phase fractionation has been shown to be particularly powerful to achieve deep proteomic libraries. We used the Spider fractionator device (PreOmics), a software-controlled rotor valve-based fraction collector coupled to a nanoflow HPLC (EASY-nLC 1000 system, Thermo Fisher Scientific), which enables the fractionation of minute amounts of material without sample loss. Here, we fractionated a total of 40 μg of purified and digested peptides that was automatically concatenated into 16 fractions using a rotor valve shift of 90 s. About 0.5 μg of each fraction were subjected to the subsequent LC-MS/MS measurements. The pre-fractionation procedures and the concatenation scheme underlying the construction of the Spider instrument have been described by us in detail (Kulak et al., 2017).

Liquid Chromatography Tandem Mass Spectrometry (LC-MS/MS) analysis

Nanoflow LC-MS/MS analysis of tryptic peptides was conducted on a Q Exactive HF Orbitrap coupled to an EASYnLC 1200 ultra-high-pressure system via a nano-electrospray ion source (all from Thermo Fisher Scientific). Peptides were loaded on a 50 cm HPLC-column (75 μm inner diameter; in-house packed using ReproSil-Pur C18-AQ 1.9 μm silica beads; Dr. Maisch). Peptides were separated using a linear gradient from 2% B to 20% B in 55 min and stepped up to 40% in 40 min followed by a 5 min wash at 98% B at 350 nl/min where solvent A was 0.1% formic acid in water and solvent B was 80% acetonitrile and 0.1% formic acid in water. The gradient was followed by a 5 min 98% B wash and the total duration of the run was 100 min. Column temperature was kept at 60°C by a Peltier element-containing, in-house developed oven.

The mass spectrometer was operated in ''top-15'' data-dependent mode, collecting MS spectra in the Orbitrap mass analyzer (6000 resolution, 300-1650 m/z range) with an automatic gain control (AGC) target of 3E6 and a maximum ion injection time of 25 ms. The most intense ions from the full scan were isolated with an isolation width of 1.5 m/z. Following higher-energy collisional dissociation (HCD), MS/MS spectra were collected in the Orbitrap (15000 resolution) with an AGC target of 5E4 and a maximum ion injection time of 60 ms. Precursor dynamic exclusion was enabled with a duration of 30 s.

QUANTIFICATION AND STATISTICAL ANALYSIS

Computational proteomics

The MaxQuant software (version 1. 6.0.12) was used for the analysis of raw files. Peak lists were searched against the human UniProt FASTA reference proteomes version of 2016 as well as against a common contaminants database using the Andromeda search engine (Cox and Mann, 2008; Cox et al., 2011). Carbamidomethyl was included in the search as a fixed modification, oxidation (M) as variable modifications. The FDR was set to 1% for both peptides (minimum length of 7 amino acids) and proteins and was calculated by searching a reverse database. Peptide identification was performed with an initial allowed precursor mass deviation up to 7 ppm and an allowed fragment mass deviation 20 ppm. For the relative quantification of MYH isoforms, only peptides unique to each isoform were used for protein quantification in MaxQuant. The relative expression of each MYH isoform is calculated as percent of the summed intensity of the four adult isoforms (MYH1, MYH2, MYH4, MYH7).

Bioinformatic and statistical analysis

The Perseus software (version 1.5.4.2), part of the MaxQuant environment (Tyanova et al., 2016b), was used for data analysis and statistics. Categorical annotations were provided in the form of UniProt Keywords, KEGG and Gene Ontology. Mitocarta2 scores were provided as numerical annotations ($x > 1$). Label free quantification (MaxLFQ) was used for protein quantification in all experiments, using Z score where indicated (Cox et al., 2014). When using pools of COX+ and COX- sections from individual patients, 100 sections were pooled, the peptides were purified and analyzed by MS in technical triplicates. This was performed in three different patients (i.e., biological triplicates, each in technical triplicates, for COX+ and COX- respectively). For the single fiber analysis, three single COX+ and three single COX- fibers were isolated from each patient (i.e biological triplicates in three patients for COX+ and COX- respectively). Comparison of quantitative parameters between the two groups was performed using Student's t-test. P-value below 0.05 was considered significant. Normalization for mitochondrial content was performed dividing expression values of each sample by the corresponding expression of citrate synthase (CS). PCA and cluster analysis was performed in the Perseus software using logarithmic expression values of LFQ. For hierarchical clustering, LFQ intensities were Z-scored and clustered using Euclidean distance for column and row clustering. The t test for the volcano plot was carried out using FDR 0.05 and 250 randomizations. Where indicated, missing values were imputed by using random numbers from a normal distribution to simulate the expression of

low abundant proteins. We used a width parameter of 0.3 of the standard deviation of all values in the dataset with a down shift by 1.8 times this standard deviation. Pathway enrichment analysis was performed using Fisher exact test with a Benjamini-Hochberg FDR cutoff of 0.02.

DATA AND CODE AVAILABILITY

The mass spectrometry proteomics data have been deposited to the ProteomeXchange Consortium via the partner repository with the dataset identifier PXD010489.

Network analysis

Functional interaction network analysis was performed using the protein-protein interaction database STRING (version 11.0). We used medium confidence (0.4), one shell of interactors and filtered interactions keeping the ones derived from experiments, textmining, database and coexpression. Protein localization was manually curated and the DAVID Bioinformatics resources (version 6.8) were used for enrichment analysis (Jiao et al., 2012).

Cell Reports, Volume *29*

Supplemental Information

Proteomics of Cytochrome *c* Oxidase-Negative versus -Positive Muscle Fiber Sections in Mitochondrial Myopathy

Marta Murgia, Jing Tan, Philipp E. Geyer, Sophia Doll, Matthias Mann, and Thomas Klopstock

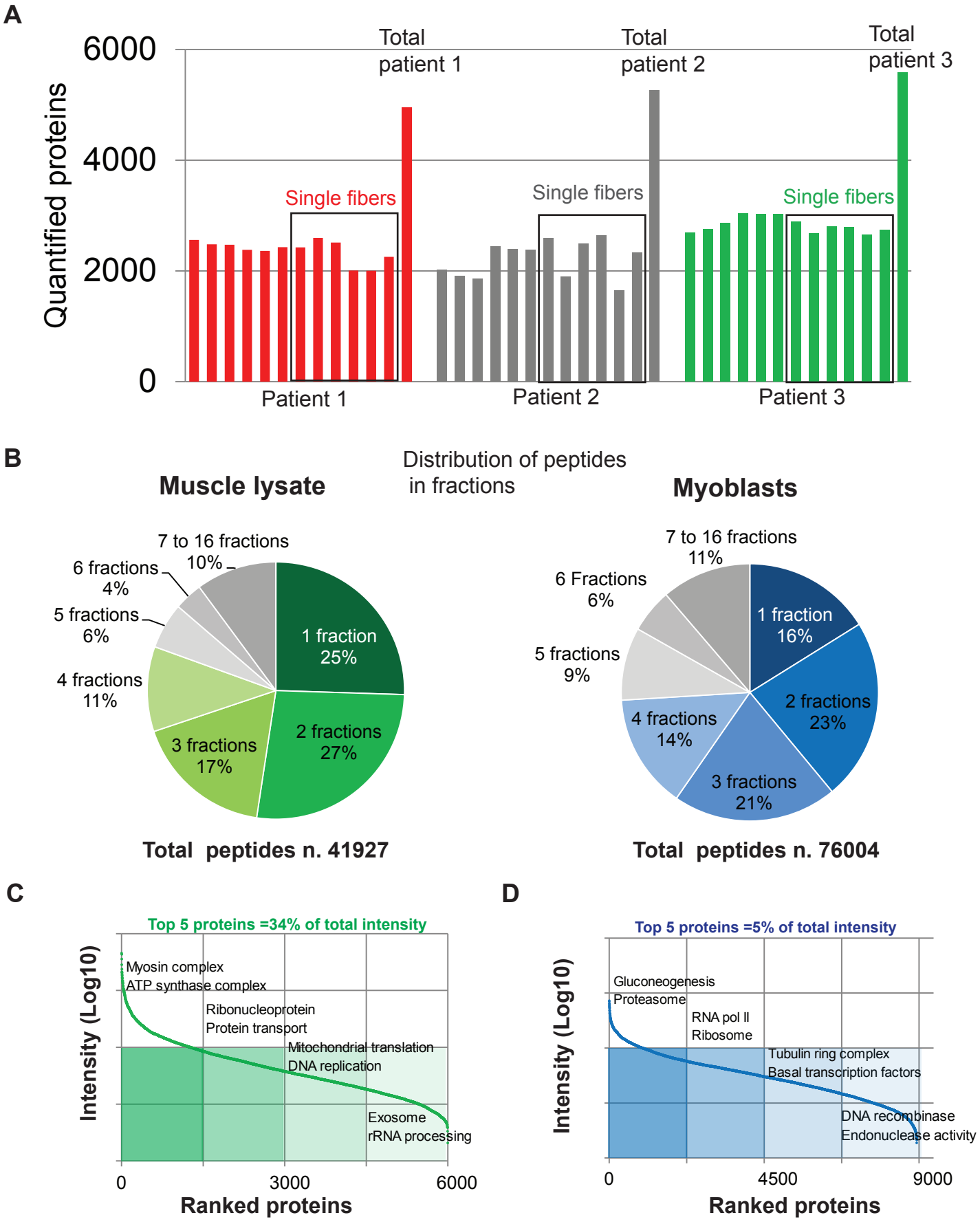

Figure S1. Protein quantification and impact of libraries.
(A) Bars show the number of proteins quantified in each patient, both in single 2 hours runs and in total, as indicated. (B) Pie charts representing the number of fractions in which a certain peptide has been detected in the total muscle and myoblast libraries. The analysis has been carried out using the numeric Venn diagram feature of Perseus. (C) Ranked intensities of all proteins quantified in the total muscle library. The data have been subdivided into quartiles. The highest annotation enrichment of each quartile (Fischer's Exact Test, FDR 0.04) is shown on the corresponding section of the grid. (D) Same analysis as in C for the myoblast library. Related to Figure 1.

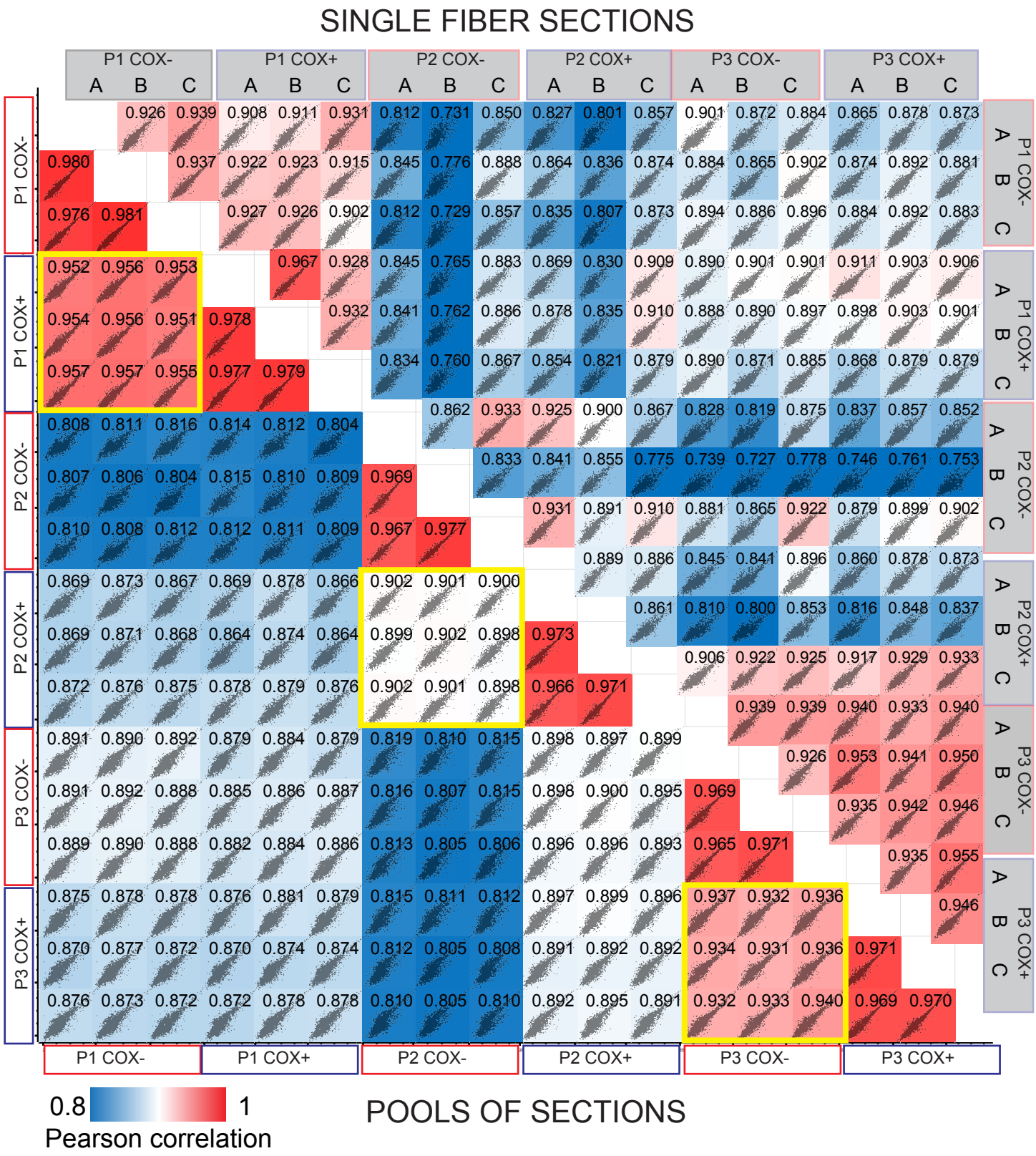

Figure S2. Multi-scatter plot matrix of correlations between all MS runs in the dataset.
LFQ intensities of fiber pools and single fibers from the three patients analyzed (P1, P2, P3 as indicated). A Pearson correlation scale ranging from 0.8 to 1 is color-coded as shown bottom right. The yellow boxes highlight the comparisons between COX+ and COX- fiber triplicates of the same patient. Technical triplicates consistently display a correlation >0.965. Related to Figure 1.

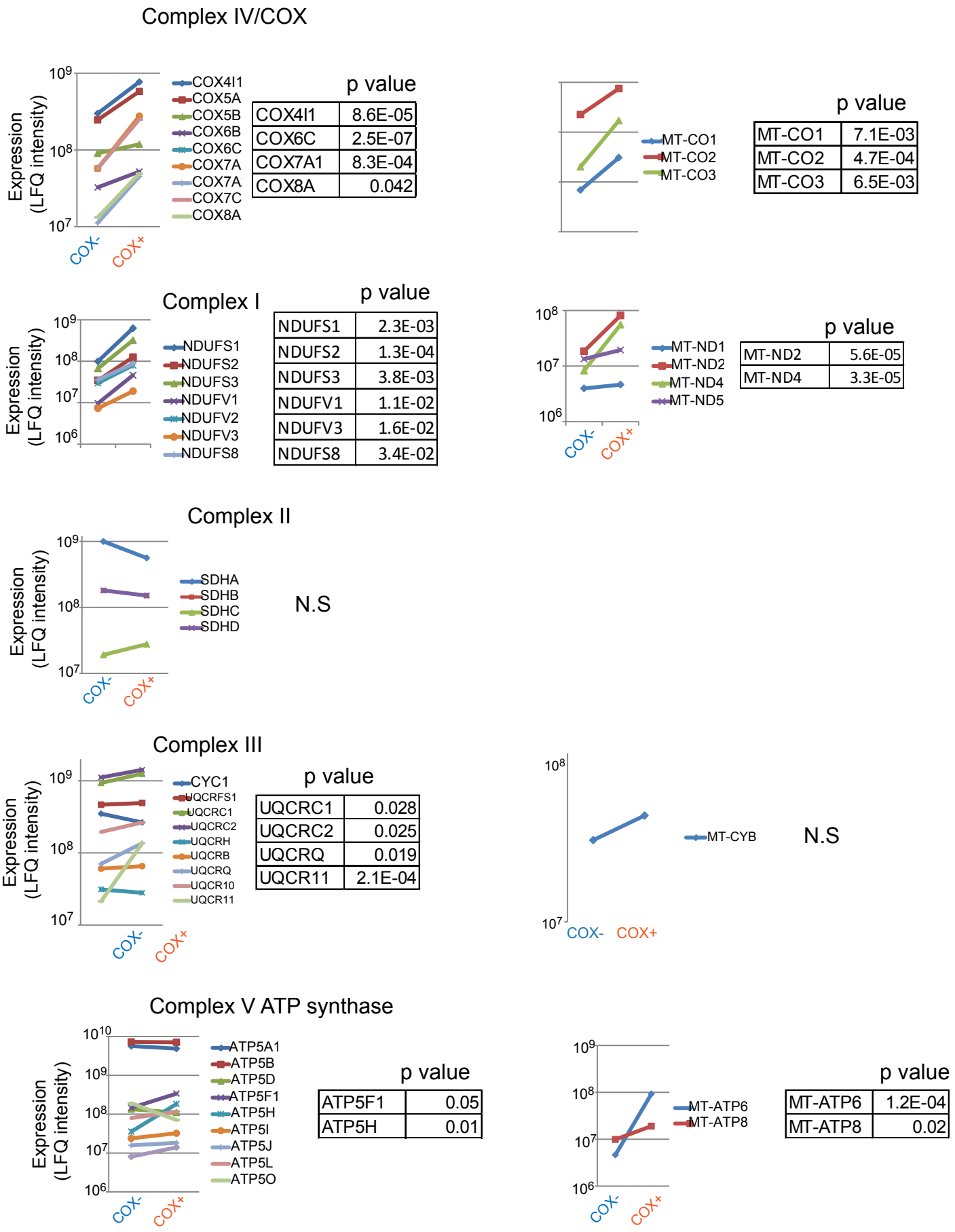

Figure S3. Line graphs comparing the expression of individual proteins of respiratory complexes between COX+ and COX- fibers.

The expression (LFQ intensity) of proteins the indicated respiratory complexes in COX- and COX+ cells. The individual proteins are listed on the right of each graph. Only the quantified core subunits of complex I are shown for simplicity. P values of Student's T-test for the indicated significant proteins in COX+ vs COX- fibers are shown on the right of each graph. Related to Figure 2.

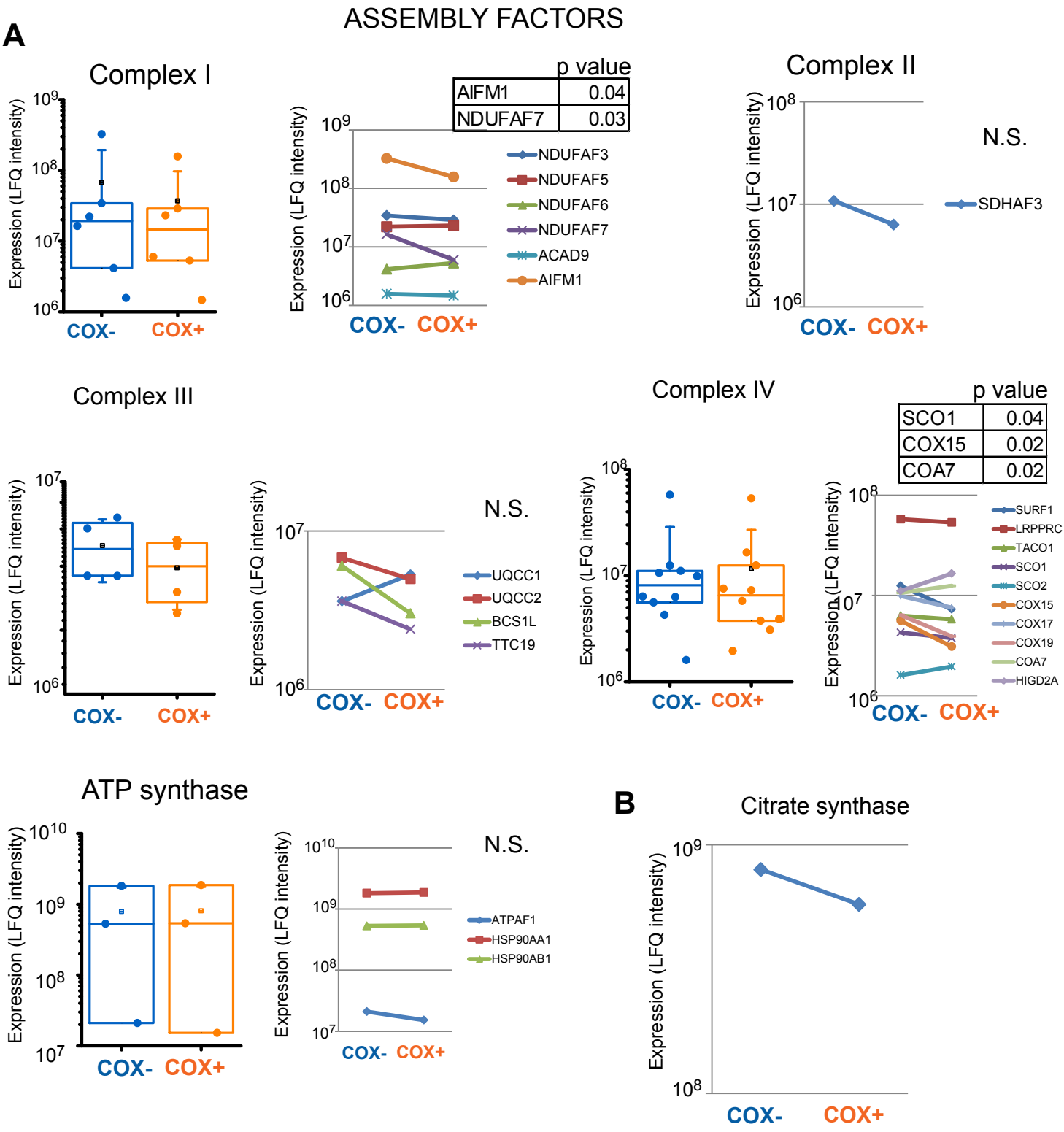

Figure S4. Expression of markers of respiratory chain assembly factors and mitochondrial content in COX+ and COX- fibers.

(A) The expression of assembly factors (which we could quantify in >75% of samples) for each respiratory complex of samples is compared in COX- (blue) and COX+ (orange) fiber pools. Boxplots are superimposed on the individual data points. Boxes show the mean, 25th and 75th percentile, whiskers show standard deviation. Line graphs next of each boxplot detail the expression of individual proteins. P values of Student's T-test for the indicated significant proteins in COX+ vs COX- fibers are shown on the right of each graph. N.S, not significant. (B) Expression of citrate synthase, a frequently used marker of mitochondrial content. Related to Figure 2.

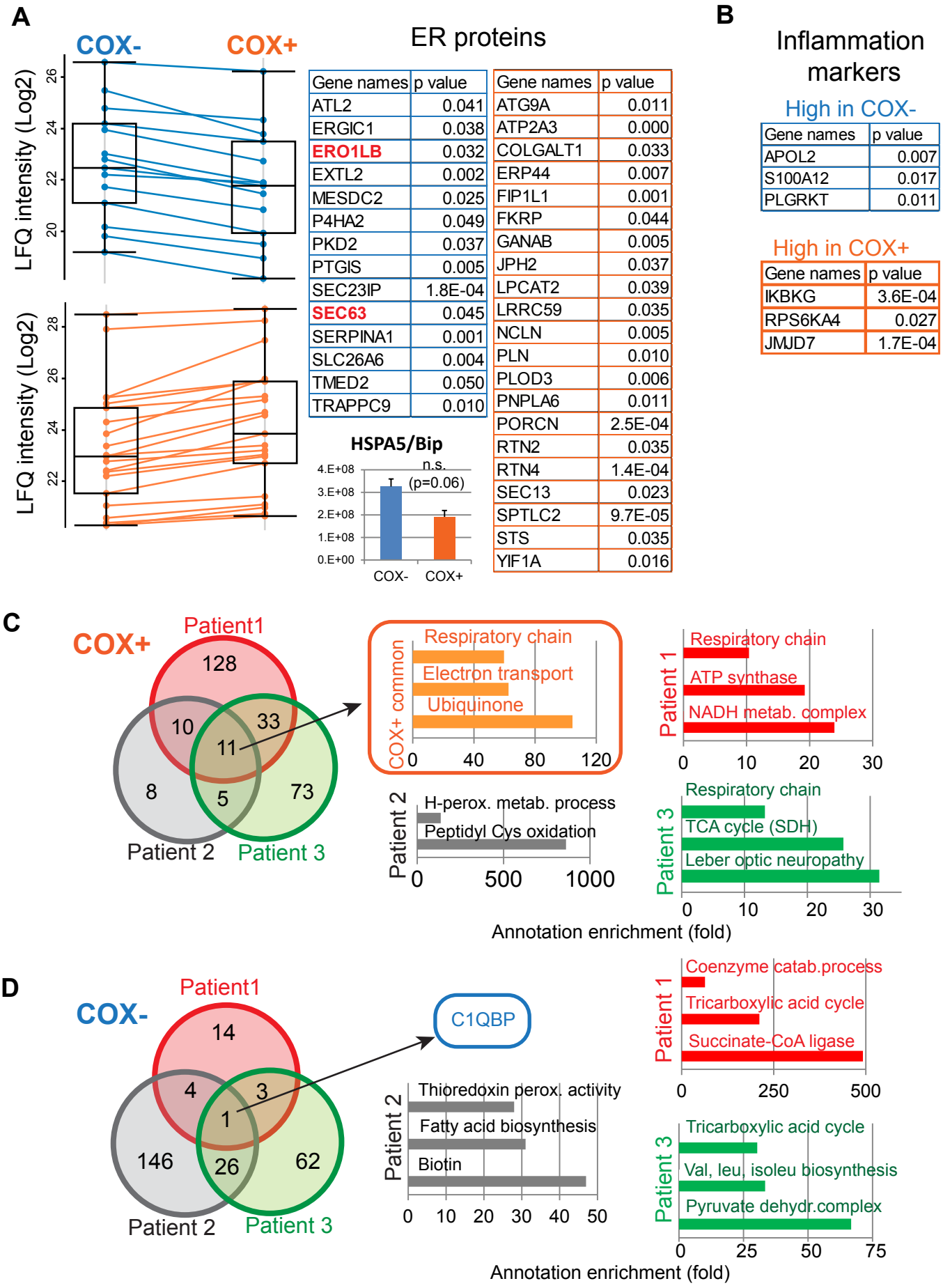

Figure S5. Endoplasmic reticulum, inflammation and mitochondrial proteome in muscle fibers of CPEO patients.
(A) Boxplot showing ER proteins with significantly higher expression in COX- (blue lines) and COX+ fibers (orange lines). The corresponding proteins and p values are indicated on the right. Proteins involved in the unfolded protein response (UPR) are marked in red. Inset, expression of the UPR chaperone HSPA5/Bip in COX+ and COX- fibers (median of three technical replicates of three patients +/- SEM). (B) List of proteins involved in inflammation with significantly different expression in COX+ and COX- fibers as indicated. (C) Analysis of patient-specific and shared features of mitochondrial disease. Venn diagram of common and patient-specific proteins displaying significantly higher expression in COX+ fibers. Highest annotation enrichments in both common and unique proteins (Fisher's exact test, FDR 0.02), are shown with the bar graphs. (D) Analysis as in (c) for COX- fibers. Related to Figure 3 and Tables S8 and S9.

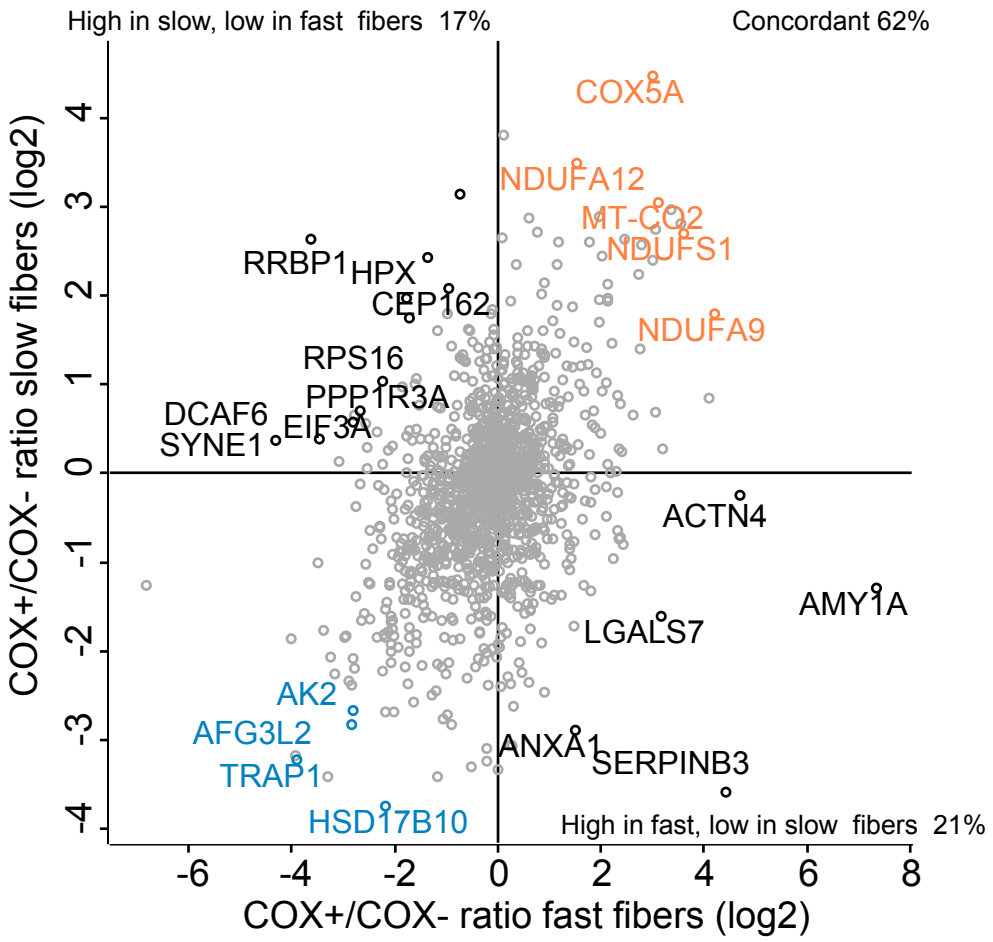

Figure S6. Differences in regulated proteins between fast and slow fibers of patient 1
The COX+/COX- ratio was calculated for each protein and slow and fast fibers were compared on a scatter plot. The fraction on proteins per quadrant was calculated to distinguish a concordant behavior (high or low in both fiber types) from a discordant one. The calculated percentages are shown. Related to figure 4.

Supplemental tables and table legends

Table S4. Basic characteristics of the CPEO patients. Related to Figure 1 and STAR Methods.

Patient code	Origin	Sex	Age at biopsy (years)	Size/heteroplasmy of single mtDNA deletion	phenotype
335-14	European-Caucasian	male	38	5 kb / 50%	CPEO
554-13	European-Caucasian	female	32	6 kb / 50%	CPEO
308-12	European-Caucasian	male	49	5 kb / 50%	CPEO

Table S5. Myosin heavy chain (MYH) composition and corresponding fiber type. Related to Figure 4.

		Pools, technical triplicates				Patient 1			**Single fibers**			**Fiber type**
%	**COX-1**	**COX-2**	**COX-3**	**COX+1**	**COX+2**	**COX+3**	**COX-**			**COX+**			
MYH7	50.3	51.2	53.0	71.1	70.6	70.6	23.8	82.1	88.7	92.1	94.0	28.5	Slow
MYH2	34.7	33.5	33.0	21.7	22.2	21.7	68.2	12.0	9.6	6.6	4.1	44.6	Fast-2A
MYH1	14.1	14.5	13.2	6.7	6.9	7.3	7.5	5.6	1.6	1.3	1.8	25.2	Fast-2X
MYH4	0.9	0.8	0.8	0.4	0.4	0.4	0.5	0.3	0.1	0.0	0.0	1.7	(Fast-2B)
		Pools, technical triplicates				Patient 2			**Single fibers**				
%	**COX-1**	**COX-2**	**COX-3**	**COX+1**	**COX+2**	**COX+3**	**COX-**			**COX+**			
MYH7	56.3	55.7	55.3	88.0	87.5	86.4	66.4	88.4	97.7	68.0	85.7	77.4	Slow
MYH2	35.6	34.3	34.8	9.8	10.0	11.1	30.1	10.6	2.1	29.9	12.2	19.2	Fast-2A
MYH1	8.0	9.8	9.8	2.1	2.4	2.4	3.5	1.0	0.2	2.1	2.1	2.9	Fast-2X
MYH4	0.1	0.1	0.1	0.1	0.1	0.1	0.1	0.0	0.0	0.0	0.0	0.6	(Fast-2B)
		Pools, technical triplicates				Patient 3			**Single fibers**				
%	**COX-1**	**COX-2**	**COX-3**	**COX+1**	**COX+2**	**COX+3**	**COX-**			**COX+**			
MYH7	55.6	54.2	52.4	66.6	68.1	67.4	30.8	91.3	89.1	84.7	92.4	85.1	Slow
MYH2	38.7	40.1	41.7	29.4	28.1	28.9	64.8	7.6	9.9	14.0	6.8	10.1	Fast-2A
MYH1	5.6	5.6	5.8	3.9	3.7	3.6	4.2	1.0	1.0	1.3	0.8	4.5	Fast-2X
MYH4	0.1	0.1	0.1	0.1	0.1	0.1	0.2	0.1	0.0	0.0	0.1	0.3	(Fast-2B)

The percent expression of each MYH isoform was calculated based on the summed intensity of the four adult isoforms of MYH COX+ and COX- fibers. This was used to assign fiber type (see Figure 4A). The expression values show individual patient samples (pool replicates and fibers) as indicated.

Table S6. Proteins involved in mitochondrial biogenesis. Related to Figure 2 and 4.

COX-	COX+	ratio	T-test Significant	p value	Valid values COX-	Valid values COX+	SEM COX-	SEM COX+	Gene names
2.7E+07	9.0E+06	3.0	+	6.7E-04	2	2	7.4E+05	2.6E+04	MTERF4
4.3E+07	2.3E+07	1.8	+	0.025	9	9	4.6E+06	2.9E+06	NOS1
8.0E+06	4.4E+06	1.8	+	0.048	6	5	9.0E+05	9.4E+05	CAMK2D
8.9E+06	5.3E+06	1.7		0.144	4	2	1.1E+06	3.3E+05	SIRT3
2.1E+07	1.5E+07	1.4		0.727	4	4	5.2E+06	3.2E+06	SSBP1
6.0E+06	5.2E+06	1.2		0.799	3	4	8.3E+05	1.6E+06	TFAM
3.1E+06	2.8E+06	1.1		0.253	5	4	1.8E+05	1.3E+05	MTO1
4.9E+06	4.5E+06	1.1		0.969	4	7	3.8E+05	1.2E+06	PRKCA
5.9E+07	6.5E+07	0.9		0.560	8	9	8.3E+06	7.5E+06	CAMK2B
8.3E+06	9.6E+06	0.9		0.748	4	5	1.9E+06	2.0E+06	PPP3CA
6.6E+07	9.2E+07	0.7		0.593	9	8	1.3E+07	1.5E+07	HCFC1
1.2E+07	1.7E+07	0.7	+	0.041	3	6	5.0E+05	3.0E+06	PRKAA2
4.3E+06	6.6E+06	0.6	+	0.030	6	6	6.7E+05	6.8E+05	MAPK1
1.1E+07	1.9E+07	0.6		0.721	6	4	6.9E+06	6.1E+06	CAMK2A
2.3E+06	5.8E+06	0.4		0.103	2	4	5.1E+05	9.0E+05	SIN3A

The LFQ expression of COX+ and COX- fibers, the COX-/COX+ ratio and the T-test p value are shown. Proteins with significantly different expression in the two groups are indicated (+). The expression values are median of technical triplicates of three patients (N=9). The corresponding standard error (SEM) is indicated.

Table S10. Proteins involved in mitochondrial fusion, fission and quality control with significantly higher expression in COX- than in COX+ slow single fibers. Related to Figure 4.

LFQ expression COX-	LFQ expression COX+	COX- /COX+ ratio	P value	SEM COX-	SEM COX+	Gene names
8.9E+07	3.4E+07	2.6	0.021	5E+07	5E+06	OPA1
7.5E+07	1.3E+07	5.6	0.007	4E+07	4E+06	AFG3L2
1.7E+08	8.1E+07	2.1	0.002	4E+07	8E+06	C1QBP
4.5E+08	1.9E+08	2.3	0.014	2E+08	2E+07	PHB
3.4E+08	1.8E+08	1.8	0.007	6E+07	3E+07	PHB2
1.7E+07	9.3E+06	1.8	0.044	5E+06	6E+05	IMMT
7.4E+07	2.3E+07	3.2	0.046	2E+07	4E+06	LONP1
7.8E+08	3.3E+08	2.4	0.027	3E+08	5E+07	HSPA9

The LFQ expression of COX+ and COX- fibers, the COX-/COX+ ratio and the T-test p value are shown. Proteins with significantly different expression in the two groups are indicated (+). The expression values are median of technical triplicates of three patients (N=9). The corresponding standard error (SEM) is indicated.

Table S11. Proteins involved in mitochondrial fusion, fission and quality control quantified in fiber pools. Related to Figure 4.

COX-	COX+	ratio	T-test Significant	p value	Valid values COX-	Valid values COX+	SEM COX-	SEM COX+	Gene names
1.3E+08	1.5E+07	8.8		0.09	6	9	5.3E+07	2.2E+07	CHCHD3
6.6E+07	1.5E+07	4.4		0.09	8	8	1.3E+07	1.0E+07	LONP1
6.6E+07	1.9E+07	3.4	+	0.01	6	8	2.9E+07	7.3E+06	AFG3L2
8.4E+08	3.1E+08	2.7		0.74	9	9	1.7E+08	3.4E+07	HSPA9
1.2E+08	4.5E+07	2.6		0.19	9	9	4.2E+07	1.7E+07	OPA1
3.7E+08	1.7E+08	2.2		0.62	9	9	8.5E+07	3.6E+07	PHB
3.2E+08	1.6E+08	2.1		0.31	9	9	5.5E+07	1.9E+07	AIFM1
1.9E+07	9.8E+06	1.9	+	0.01	3	2	1.1E+06	1.0E+06	YME1L1
5.6E+07	3.0E+07	1.9	+	0.01	3	3	7.1E+06	1.7E+06	IMMT
8.9E+06	5.3E+06	1.7		0.14	4	2	1.1E+06	3.3E+05	SIRT3
1.3E+07	8.1E+06	1.6		0.13	7	9	2.0E+07	4.0E+06	HSPE1
3.4E+08	2.2E+08	1.5		0.98	9	9	6.0E+07	4.2E+07	PHB2
1.1E+08	7.9E+07	1.4		0.11	9	9	3.0E+07	1.1E+07	C1QBP

7.7E+08	5.5E+08	1.4		0.93	9	9	1.3E+08	6.1E+07	VDAC2
6.8E+08	5.2E+08	1.3		0.15	9	9	1.3E+08	5.0E+07	PRDX3
7.5E+07	5.8E+07	1.3		0.17	6	6	1.3E+07	1.5E+07	FIS1
5.1E+07	4.3E+07	1.2		0.23	7	9	2.4E+07	1.0E+07	APOOL
6.3E+06	5.8E+06	1.1		0.25	3	2	3.9E+05	2.9E+05	MAP1LC3B
2.6E+08	2.4E+08	1.1		0.20	9	9	4.6E+07	4.1E+07	VCP
2.2E+08	2.2E+08	1.0		0.58	9	9	3.9E+07	4.1E+07	CYCS
7.7E+06	8.0E+06	1.0		0.72	4	6	4.4E+05	8.6E+05	SQSTM1
2.0E+06	2.1E+06	0.9		0.35	2	5	1.7E+05	2.9E+05	NPLOC4
9.3E+05	1.1E+06	0.9	+	0.04	3	2	3.7E+04	2.0E+04	HTRA2
2.4E+06	3.1E+06	0.8		0.94	3	3	5.3E+05	6.1E+05	BNIP3
4.9E+06	6.3E+06	0.8		0.25	3	5	3.5E+05	5.3E+05	MFF
1.3E+08	2.0E+08	0.7	+	0.02	8	9	2.0E+07	1.9E+07	HUWE1
3.6E+06	5.4E+06	0.7		0.48	5	6	1.4E+06	6.0E+05	MFN2
1.3E+06	2.0E+06	0.6		0.30	3	3	1.8E+05	2.8E+05	GABARAPL2
1.0E+07	2.0E+07	0.5		0.16	9	7	3.0E+06	6.6E+06	DNM1L
1.3E+07	5.7E+07	0.2	+	6.2E-05	6	3	1.5E+06	8.7E+05	SH3GL1

The LFQ expression of COX+ and COX- fibers, the COX-/COX+ ratio and the T-test p value are shown. Proteins with significantly different expression in the two groups are indicated (+). The expression values are median of technical triplicates of three patients (N=9). The corresponding standard error (SEM) is indicated.